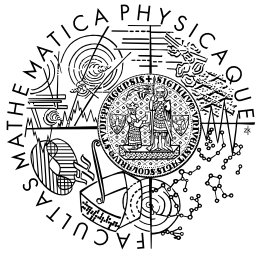

FACULTY
OF MATHEMATICS
AND PHYSICS
Charles University

MASTER THESIS

Juraj Májek

Evaporation of simple and complex fluids at different surface wettability

Department of Macromolecular Physics

Supervisor of the master thesis: RNDr. Artem Ryabov, Ph.D.

Study programme: Physics

Study branch: Physics of Condensed Matter and Materials

Prague 2022

I declare that I carried out this master thesis independently, and only with the cited sources, literature and other professional sources. It has not been used to obtain another or the same degree.

I understand that my work relates to the rights and obligations under the Act No. 121/2000 Sb., the Copyright Act, as amended, in particular the fact that the Charles University has the right to conclude a license agreement on the use of this work as a school work pursuant to Section 60 subsection 1 of the Copyright Act.

In ..... date ....

Author's signature

I would like to thank the many people that made the completion of this thesis possible: first of all to my wonderful supervisor RNDr. Artem Ryabov, Ph.D., for all your patient guidance, for all your contacts you inquired when we were unsure with something, for the many corrections and revisions you did that helped push this work to a higher level, and for all the assistance you provided me throughout my whole study.

I would like to thank my consultant Doc. RNDr. Ondřej Kylián, Ph.D. for supervising my laboratory work. I am much obliged to Mgr. Anna Kuzminova, PhD. for preparing all the surfaces and enduring the cold in the SEM room with me. I would like to thank our biophysicists Mgr. Alžbeta Kuižová and RNDr. Eva Kočišová, PhD. for preparing the liposomes, doc. RNDr. Helena Valentová, Ph.D. for teaching me how to work with the microscope, and our mathematicians RNDr. Michal Pavelka, Ph.D. and Mgr. Ondřej Kincl for their work on the SPH simulations.

I am deeply grateful for my family, for my mom, for my dad, for Mišo and for Evka and Zuzka. For all the care you have given me, each in their own way. For supporting me through my studies and all of my life, for supporting me in who I chose to become. Thank you from all my heart. I would also like to thank my friends which I met on the journey, who encouraged me to carry on, and partly became a family of mine too.

I would like to dedicate this thesis to my beloved fianceé Anežka. Thank you for inspiring me, for bearing with me through all the highs and lows and loving me so much. I love you too, and look forward very much for spending my life with you. Particularly, I would like to thank you for reminding me that, both droplets and our lives, even though they are can be messy, tedious and often don't behave as planned, are ever beautiful and precious. May we never forget that.

To express both this beauty and my gratitude to all of you, I would like to share my favourite image shot during the work on this thesis: the *T-rex shooting lightning from his arms while standing on a droplet*, see Fig. 1.

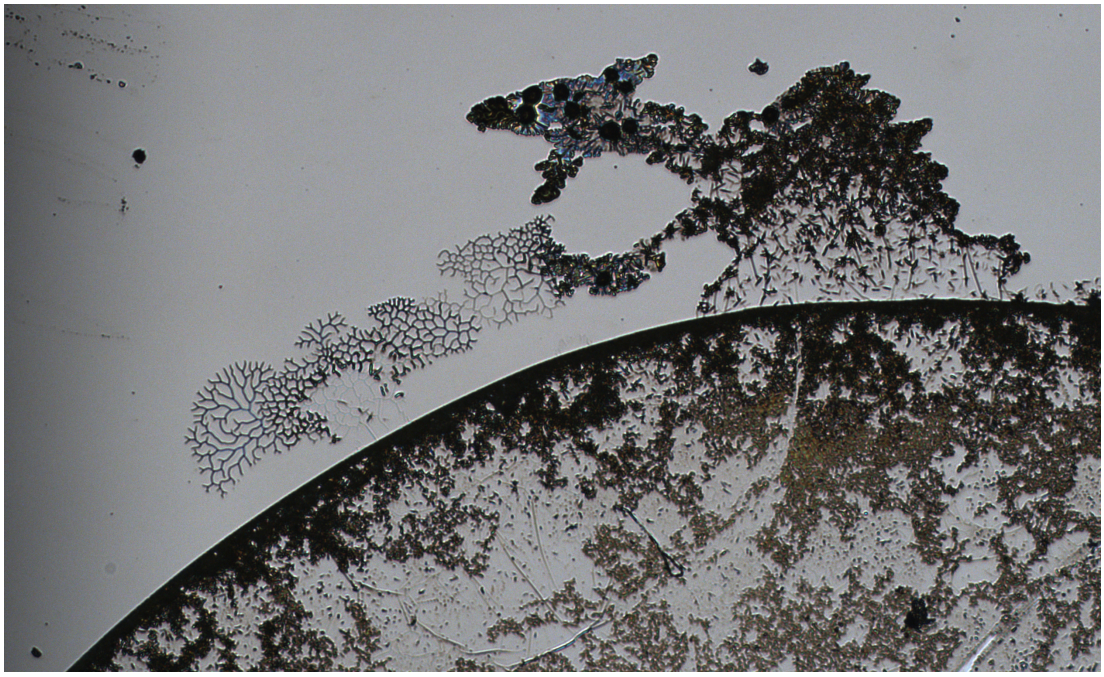

Figure 1: T-rex shooting lightning from his arms while standing on a droplet. A proof that soft matter physics can be dangerous business. Luckily, this one was friendly. Liked to sunbath in the microscope lamp. A deposit created by a 4μl droplet with riboflavin at concentration 0.1mg/ml evaporating on a scratched, old PTFE/Si surface at 30°C. Captured with magnification 5×.

Title: Evaporation of simple and complex fluids at different surface wettability

Author: Juraj Májek

Department: Department of Macromolecular Physics

Supervisor: RNDr. Artem Ryabov, Ph.D., KMF MFF UK

Abstract: In this work, we investigate the evaporation dynamics of sessile droplets in two scenarios: (i) droplets evaporating on Teflon plasma polymer coated surfaces, exhibiting anomalously long evaporation lifetime for their size, (ii) drying droplets with liposome suspensions that gradually spread while evaporating.

(i) By observing water droplets evaporating on a silicon wafer coated with a Teflon thin film, we discover that the water disintegrates and penetrates the Teflon film. The droplets hide some of their volume underneath, which then does not evaporate. This leads to anomalously long evaporation times. We attribute this effect to structural instability of the Teflon layer, stemming from the contact of non-polar Teflon and polar SiO_2. By using Teflon surfaces at most week old, this effect can be prevented. We further identify and describe typical features of the penetration, allowing for its early detection.

(ii) We measure the spreading of liposome-laden droplets and find an increase of radius up to 30% of the initial value. During the increase, the droplet contact line spreads in bursts, or protrusions, not uniformly. Existing literature shows that liposomes adsorb on both the air/water and the water/surface interface and reduce the corresponding surface tensions γ_{gl} and γ_{sl}. We find that when the adsorption of the liposomes to a hydrophobic surface lowers γ_{sl}, the advancing contact angle changes in a way that may induce spreading.

Keywords: sessile droplets, evaporation, wetting, liposome

Contents

Introduction

Falling from the sky during rain, condensing on grass after the morning dew, trailing down our cheeks when we cry, no fluid form is as poetic as the droplet. Sessile droplets are also of great importance for industry [1], medicine and diagnostics, and it is vital for these applications that the processes within the droplets are well understood. Examples of the applications include: (i) novel printing technologies [2], where the wetting, evaporation and adsorption properties are vital for the stability of the print, (ii) lab-on-chip applications [3], where the small volume of the droplets allows for efficient fast mixing, and the droplet acts as a microreactor, (iii) nanoparticle self-assembly [4, 5], where by controlling the evaporation conditions one can create specific patterns of deposits left behind by an evaporating droplet, (iv) chemical or biological analysis: the flows within the droplet can concentrate a solute, allowing for detection of dilute contaminants [6, 7], or they can sort different types of cells or particles of different sizes [8]. Furthermore, the morphology of the deposit can be used for automatic disease diagnostics [9].

The evaporation of a pure water droplet is a complex process [10]. The droplet shape is determined by gravity, the surface tensions of the interfaces involved, and the morphology of the surface upon which the droplet sits, its various irregularities acting as pinning points for the droplet contact line. The droplet shape then determines the inhomogenous evaporation profile across the droplet surface [11] and can induce radial flows within the droplet volume [12]. These flows compete against circulating ones induced by temperature and surface tension gradients [13, 14].

The droplet shape and the flows during the evaporation can be controlled by the surface used, namely by its hydrophilicity or hydrophobicity. The simplest example of hydrophilic surface is the silicon wafer covered with silicon oxide layer created due to oxidation in air. The wafer is often coated with Teflon plasma polymer to create a simple hydrophobic surface [15]. However, as we show in this thesis, this surface is not simple at all, and the interactions between its layers and the water droplet can result in a spectacular evaporation regime and extremely long evaporation times.

The complex behavior of liquid flows during droplet evaporation can be utilized for preparing samples for spectroscopy. When molecules are dissolved or particles added to the droplet, they are carried with the flow inside. The resulting deposit that remains after the water vaporizes carries information about the flows [14]. Common is the formation of the so-called Coffee Ring [12], where the solute of the droplet accumulates at the droplet edge, carried by the radial flow. The solute is therefore greatly concentrated in the ring-like structure, allowing for detecting of very diluted substances within the droplet.

The situation becomes more involved if the droplet contains surface-active molecules (surfactants). These can adsorb on the air/water or the water/solid interfaces [16, 17, 18] and modify the respective surface tension, which in turn modifies the flow. This creates a feedback loop between the surfactant distribution in the droplet and the flow within, resulting in remarkable evaporation dynamics [19, 20, 21].

In this thesis, we describe and explain a remarkable effect that appeared during sample preparation for spectroscopy, which was exhibited by liposome-laden droplets. Namely, when evaporating, at some point the droplets can start spreading, expanding on the surface though their volume decreases. Experimental observation of such a spreading was reported apparently for the first time in [22], however, a systematic study and understanding which molecular interactions are relevant is still lacking. Here, we investigate this effect in a quantitative way and present possible theoretical explanations.

Contents

Chapter 1 explains the basic processes that guide droplet spreading: how the droplet shape is formed from the balance of forces acting on it and how this shape influences the flows within the droplet. In Chapter 2, we investigate complex interactions of droplets with the surface: for some multilayered surfaces the droplet can penetrate the top layer and hide beneath, resulting in very prolonged evaporation. Chapter 3 explains the experimental setup used to gain quantitative data from the evaporation process and presents the data from measured spreading liposome-laden droplets. Chapter 4 reviews the literature concerning the effect of liposomes on surface tension and investigates possible explanations: we first assumed the measured spreading is caused by adsorption of liposomes to the air/water interface only. However, it turns out that we need to include also the adsorption of liposomes on the surface. The thesis contains also one Attachment displaying the code used for automatic processing of droplet shape data sequences.

1. Theoretical foundations of droplet evaporation

In this Chapter, we shall discuss the basic physical laws governing the droplet statics and dynamics which are relevant for this work. At first, we will explain how the forces acting on the droplet sculpt its shape. Following that we will discuss the many processes happening during droplet evaporation.

1.1 Sessile droplet shape

Droplet in a gravitational field assumes a shape that is given by the interplay of gravitational force and surface tension. These two determine the relevant length scale, called capillary length:

$$\lambda_c = \sqrt{\frac{\gamma}{\rho g}}, \tag{1.1}$$

where g is the gravitational acceleration, γ the surface tension of the liquid-air interface and ρ the density of the liquid. Small droplets assume a shape that is approximately a spherical cap, but they cannot be higher than capillary length [23]. Larger droplets that would be too high in a spherical shape instead flatten into so-called 'macrodroplets', or commonly reffered to as puddles, see Fig. 1.1. For water on Earth's surface, the value is about 3mm. Droplets studied in this work were generally smaller than this and could be approximated by a spherical cap.

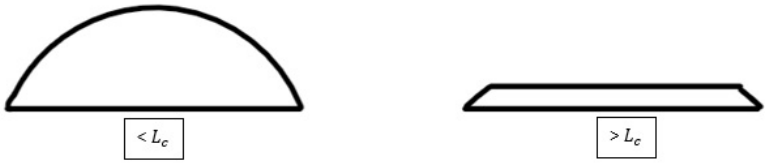

Figure 1.1: Microdroplet (left) with the length and height lesser than λ_c and a macrodroplet (right) with length higher than and height equal to λ_c (the two are not to scale). Taken from [24] with permission.

Contact angle

The most relevant quantity for droplet shape and behaviour is not its height, but its contact angle θ, defined as the angle with which the droplet's surface touches the surface. On an ideal smooth surface, this angle is determined by the balance of surface tensions between the three phases, resulting in the Young's relation:

$$\cos\theta = \frac{\gamma_{sg} - \gamma_{sl}}{\gamma_{gl}}, \tag{1.2}$$

where γ_{sl} denotes the surface energy of the solid-liquid interface, and γ_{sg} and γ_{gl} the energies of the solid-gas and gas-liquid interfaces, respectively.

Hysteresis

On rough surfaces, the above relation does not hold absolutely. Instead of a precise allowed contact angle value, there is an allowed range of angles. Usually, if one would pump more water into the droplet, it would immediately expand with a constant contact angle. For a rough surface, however, the contact line can become pinned by a defect on the surface. This defect will then exert a force f to keep the contact line static.

The force balance given by (1.2) is then modified by this force, resulting in:

$$\cos\theta = \frac{\gamma_{sg} - \gamma_{sl} + f}{\gamma_{gl}}. \tag{1.3}$$

Thanks to this, the droplet will, instead of advancing, adopt a higher contact angle. The same holds for when one pumps water out from a droplet: the droplet will adopt a lower contact angle. Overall, there is a maximum force that the defects can exert on the contact line, which results in a maximum/minimum contact angle allowed. If these would be exceeded, the droplet will start to advance/recede, and therefore the angles are called *advancing* and *receding* contact angles, θ_A and θ_R, see Fig. 1.2.

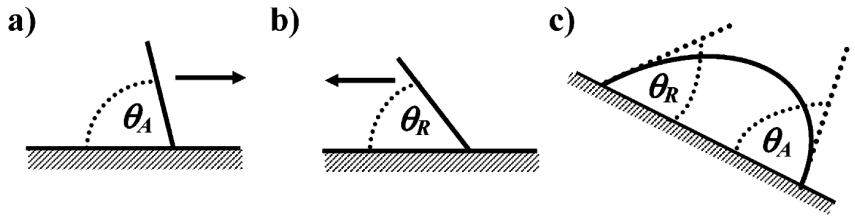

Figure 1.2: A schematic showing the advancing (a), receding (b) contact angle and the way to measure them at the same time at a tilted surface (c). Adapted with permission from [25]. Copyright 2014 American Chemical Society.

Contact angle determination

In principle, the contact angle can be determined simply by fitting a tangent line to droplet surface from a photo. However, much more accurate is to fit the entire spherical cap of the droplet. In this work, we have used two methods developed in [26, 27], with code freely available in [28].

The first one is called Low-Bond Axisymmetric Droplet Analysis (LBASDA) [26], that fits an analytic solution to Young's equation via a first-order perturbation technique. It interpolates the droplet profile from the image to reach subpixel resolution. For automatic fitting, it requires the user to input γ_{lg} of the liquid, which was in general not known in our case and therefore it was done manually (by altering the parameters of the fitting curve until it fit the droplet shape).

The second one is called DropSnake [27]. It fits the droplet contour with multiple splines elastically linked to each other, which ensures the splines obey the Young's equation. This technique is faster and fits the profile automatically without no further input. Further automatization procedure was developed in this work that allows for analysis of the droplet in its entire lifetime, consisting of $500 - 1000$ snapshots. This is described in the manual downloadable at [28].

Both techniques are able to fit only the real droplet contour, or both the real one and its reflection in the surface, which allows for more precise results.

1.2 Evaporation dynamics

The evaporation process involves multiple environments and multiple scales. It is influenced by the air around the droplet, by its humidity and the presence or absence of wind. The evaporation rate and the distribution of evaporation flux depend on the droplet shape. This shape, in turn, is given by the forces at the droplet contact line, to which contribute also forces from microscopic defects. Due to this multiscale structure, two droplets rarely evaporate in an exactly same way. We shall here consecutively explain the basic physics at work on each of scales.

1.2.1 Droplet shape dynamics

On a rough surface, the initial angle of the droplet is larger than the receding angle. Because of this, the contact line remains pinned and the droplet evaporates with a *Constant Contact Radius (CCR) mode*. The contact angle decreases until it reaches θ_R.

As the droplet further evaporates, the angle cannot decrease any more and the droplet will start receding, as the force from the defects is no longer sufficient to hold it in place. This is called the *Constant Contact Angle (CCA) mode*.

In its final moments, the droplet is already too small and the evaporation too fast for the droplet to evaporate in a steady-state regime, and therefore both contact angle and contact radius decrease in what is called the *Mixed mode*, until all liquid in the droplet evaporates. For an example of the dynamics, see Fig. 1.3.

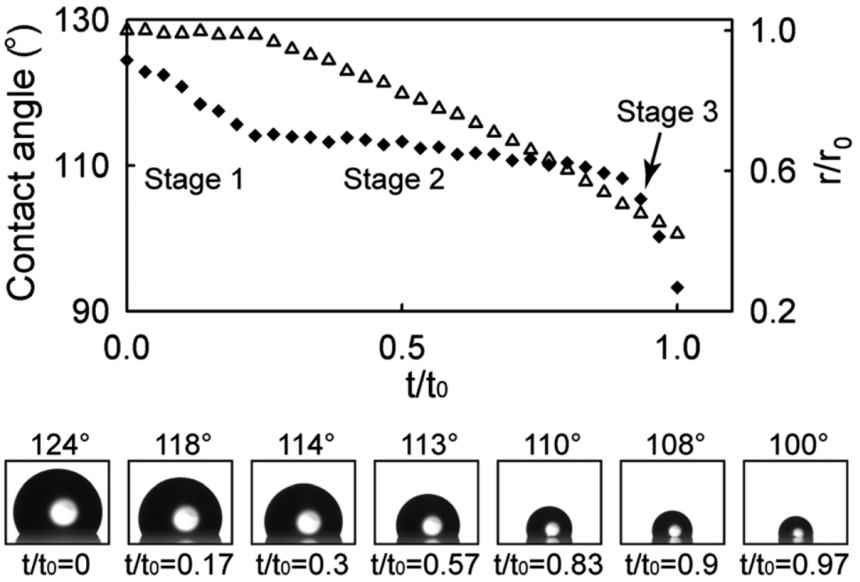

Figure 1.3: An example of the droplet shape evolution. First, the droplet evaporates with a pinned contact line in the Constant Contact Radius (CCR) mode, where only the contact angle decreases. When it reaches θ_R, it starts to recede in the Constant Contact Angle mode (CCA). At last, it becomes too small to equilibrate properly and both quantities decrease in the Mixed Mode. Reproduced from Ref. [29] with permission from the Royal Society of Chemistry.

1.2.2 Evaporation profile

The evaporation of droplets at room temperature is a slow process, their lifetime being minutes to tens of minutes for microlitre-droplets. While evaporating in ambient conditions with no wind, the droplet dynamics is in a steady state . This results in steady diffusion of the vapor away from the droplet, obeying the steady-state diffusion equation, i.e. Poisson's equation for concentration of the water vapour c:

$$\Delta c = 0. \tag{1.4}$$

The boundary conditions for the process are as illustrated in Fig. 1.4, where on the dry substrate a von Neumann condition is applied and constant concentrations are imposed on the surface of the droplet and in infinity. The von Neumann conditions can also be satisfied using the mirror method as in electrostatics, solving a problem where everything is mirrored with respect to the substrate.

The quantity of interest is, however, not directly the concentration profile of water vapour, but the flux of the vapour going away from the droplet surface $\vec{J}$, which obeys the Fick's law with vapour diffusion constant D:

$$\vec{J} = -D\nabla c. \tag{1.5}$$

Ideal droplets have the shape of an axisymmetric spherical cap, hence $\vec{J}$ on droplet surface depends only on the azimuthal angle ϑ. Equation (1.4) can be solved analytically for any contact angle, resulting in the evaporation flux field [30]:

$$J(\vartheta) = \frac{C_s - C_\infty}{R} F(\vartheta, \theta, R), \tag{1.6}$$

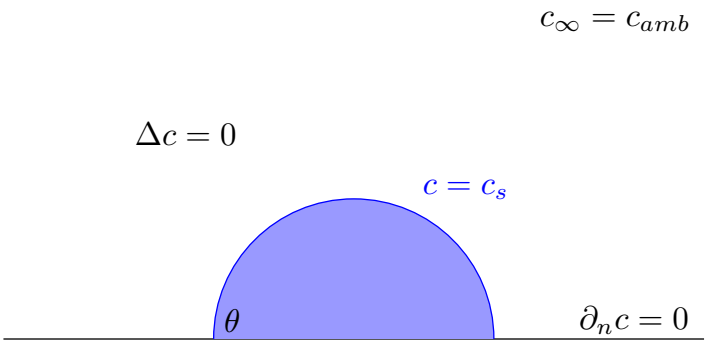

Figure 1.4: Problem setting for the Laplace's equation governing the droplet evaporation. Water vapour concentration at infinity is the ambient concentration c_{amb}. At droplet surface, concentration is at saturation level c_s. At the surface layer, von Neumann conditions are imposed. Solving the Laplace equation for c, one can obtain the evaporation flux J as $J = -D\nabla c$. The flux at droplet surface solved analytically can be found in [30].

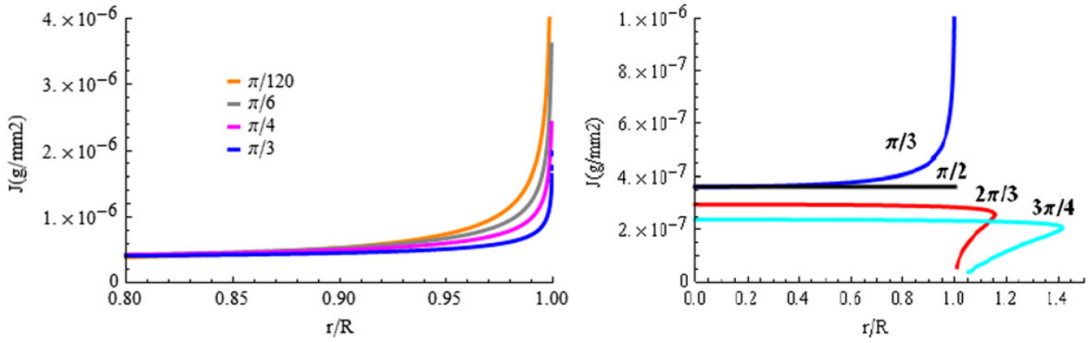

Figure 1.5: The evaporation flux profile across the droplet for different acute (left) and obtuse (right) contact angles, derived in [30]. It can be seen that the flux is constant over the whole droplet for $\theta = 90°$. For $\theta < 90°$, it diverges near the contact line. For $\theta > 90°$ it approaches zero near the contact line. Adapted with permission from [30]. Copyright 2012 Elsevier.

where C_s is the saturation water concentration, C_∞ the ambient water concentration at infinity, R the wetted radius of the droplet and F is a function whose the exact form can be found in [30]. The resulting evaporation profiles can be seen in Fig. 1.5. When we integrate $J(\vartheta)$ across the whole droplet surface, we receive the overall evaporation flux, $E(t) = -dV/dt$. During the first stage of the evaporation with a pinned contact line, $E(t)$ is approximately constant, and the volume decreases linearly. In the second stage, with a constant contact angle, it holds approximately that $V^{2/3} = V_0^{2/3} - kt$ [30].

1.2.3 Flows within the droplet

Outward flow & Coffee ring effect

The diverging evaporative flux at lower contact angles (shown in Fig. 1.5 (left)) means that much more liquid is lost at the edges of the droplet than at its apex. When the contact line is pinned, liquid must therefore be transported from the centre of the droplet to its edge to keep it from receding [12]. This leads to a radial outward flow from the droplet centre to its edge, illustrated in Fig. 1.6.

If the liquid of the droplet is a suspension or solution, the material within is also transported to the edge by the flow. In most cases, it cannot evaporate and instead sediments on the substrate at the droplet edge, or is adsorbed at the droplet surface near the edge [31]. The exact ratio of these two effects is not generally known, but when all of the droplet liquid evaporates, the resulting sediment is greatly concentrated at its circumference, resulting in a ring-like stain giving the effect its name, *Coffee ring effect* [12]. As the particles accumulate at the contact line due to the radial flows, they provide additional defects, strengthening the contact line hysteresis [32]. A droplet containing nanoparticles, for example, can stay pinned during its entire evaporation due to ever stronger hysteresis, even on surfaces which normally have little roughness. See Chapter 3 for our own results documenting this.

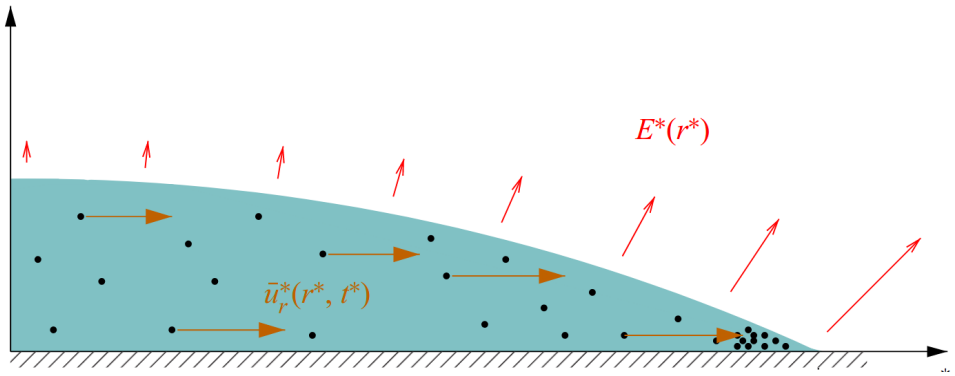

Figure 1.6: A droplet with acute contact angle, with evaporation flux E diverging at droplet edge. This divergence leads to outward radial flow u, which transports particles within the droplet to the edge, where they accumulate. Adapted with permission from [33]. Copyright 2021 Cambridge University Press.

Marangoni forces & Circulatory flow

From the above reasoning, one would think that all droplets with a pinned contact line create coffee rings, which is not true as was found by Hu & Larson in [14]. The authors of this paper have found a counteracting effect creating a flow suppressing the formation of coffee rings. Since the droplet is cooled by evaporation, it is colder than the surrounding air and the surface upon which it sits. The surface is at constant temperature and supplies heat back to the droplet, which creates a temperature gradient across its volume: the further from the surface, the colder the droplet is. For an example temperature profile, see Fig. 1.7.

Many material properties are temperature dependent and among them is also the surface tension γ_{gl}. The temperature gradient, therefore, induces a surface

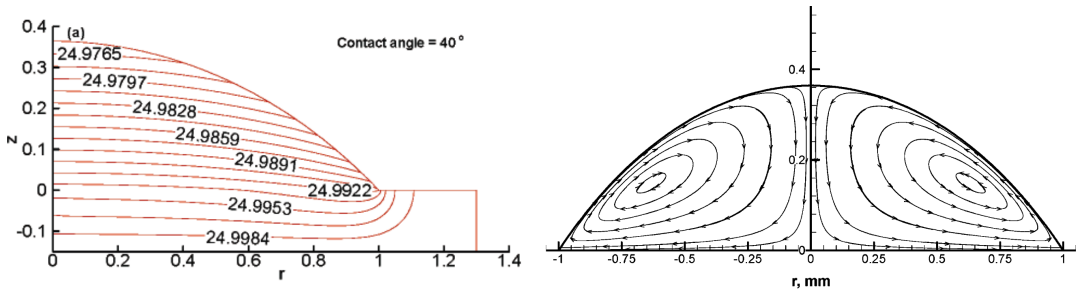

Figure 1.7: Circulating Marangoni flow inside a droplet (right) and its source, the temperature gradient (left). It can be seen that the top of the droplet is colder due to evaporation, which results in the circulatory flow. Both fields were computed using a FEM simulation in [13]. Adapted with permission from [13]. Copyright 2005 Americal Chemical Society.

tension gradient. Gradients of surface tension create a force, called Marangoni force, seen daily when washing dishes and dropping a drop of liquid soap into water. In the droplet, Marangoni force creates circulating flows as seen in Fig. 1.7. These flows compete with the radial ones and can overcome the coffee ring effect, as documented first in [14].

2. Prolonged evaporation on permeable surface

The standard time for a 2μl droplet to evaporate in room conditions is under 20min. Some droplet in our experiments evaporating on PTFE/Si surfaces (see Sec. 3.2 for details on the surfaces used) took an overwhelmingly longer time to evaporate fully, the records being over 2 hours, which was highly impractical for experiments.

For given values of ambient humidity and temperature, of initial volume, initial contact angle and receding contact angle, lifetime of an evaporating water droplet was calculated by Nguyen et al. in [34]. The 2 hour droplet lifetimes we observed do not obey their calculations. The same authors show, in [35], that introducing nanoparticles to the droplet can reduces the lifetime, but only by pinning the contact line. Kim et al. in [36] show that for very concentrated coffee suspensions, lifetime increases for higher fraction of coffee in the suspension (up to 80% of coffee). We have, however, observed prolonged evaporation also for pure water droplets, so these works cannot explain our observations.

We set to investigate the prolonged evaporation process using light microscopy as described in Sec. 3.3. We observed the evaporation of both pure water droplets and solutes of riboflavin, which was chosen as a simple non-surfactant molecule forming visible aggregates.

2.1 Initial observations: strange patterns

We have discovered that all the droplets that exhibited anomalously long lifetimes also had a pinned contact line during the whole evaporation process. In the microscope we saw these droplets exhibit astonishing features unseen for normally evaporating droplets. Observing riboflavin-laden droplets allowed us to see these features better and to also see their effect on the deposits. The four different features we identified can be seen in Fig. 2.1 and 2.2:

1. Branching tunnels extending both inside and outside the droplet, shown in Fig. 2.1 (left column). These grew and shrunk in a pulsating manner during evaporation. When the droplet evaporated fully, traces of them were left in the deposit (Fig. 2.1 (e)).

2. Pockets as in Fig. 2.1 (right column), appearing first circular in shape, which then merged and after evaporation left behind a net of filament-like deposits.

3. Hives as in Fig. 2.2 (a)-b)). These were visible only in the deposits and always appeared in the droplet centre.

4. Outer rings as in Fig. 2.2 (c)-d)). These always had elliptical shape reaching beyond the droplet bulk. They contained smaller particles than the average in the bulk droplet.

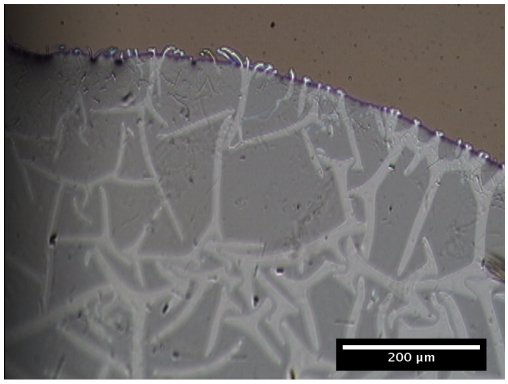

(a) Droplet A, $t = 1075$s.

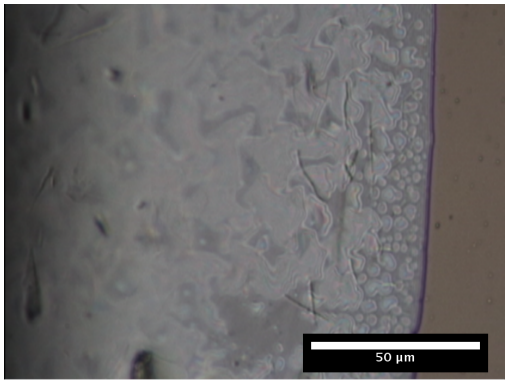

(b) Droplet b, $t = 6229$s.

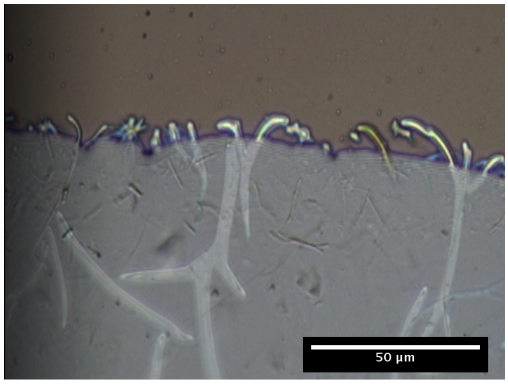

(c) Droplet A, $t = 1285$s.

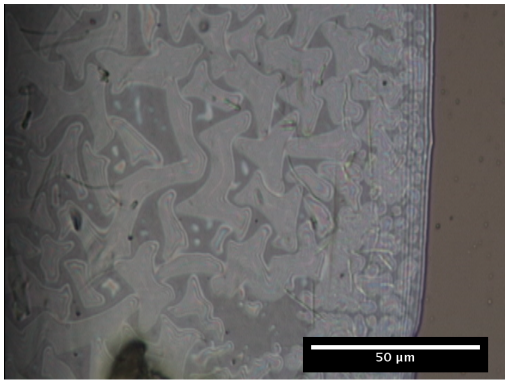

(d) Droplet B, $t = 7123$s.

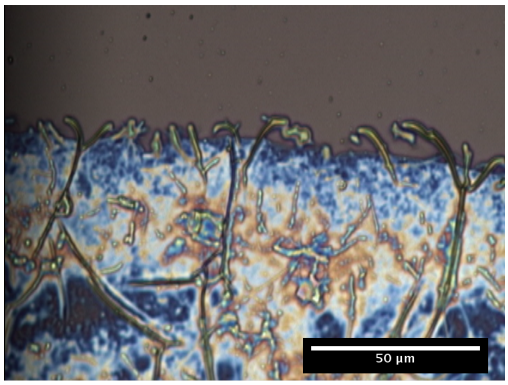

(e) Droplet A, $t = 2078$s, dry.

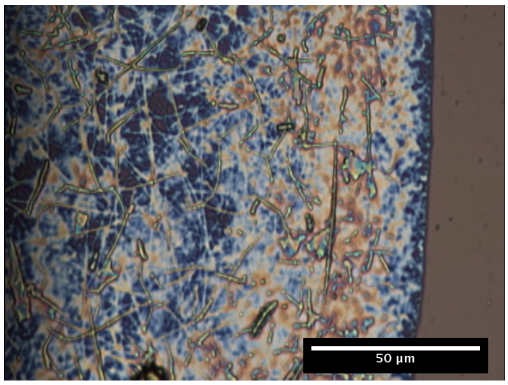

(f) Droplet B, $t = 7253$s, dry.

Figure 2.1: Two of the typical features of the penetrating droplets: branches (left) and pockets (right). The images are taken from two separate droplets, both of which were 0.1mg/ml solution of riboflavin with volume 4μl evaporating on a PTFE/Si surface in 30°C. The surface was about one year old and stored on air before using it.

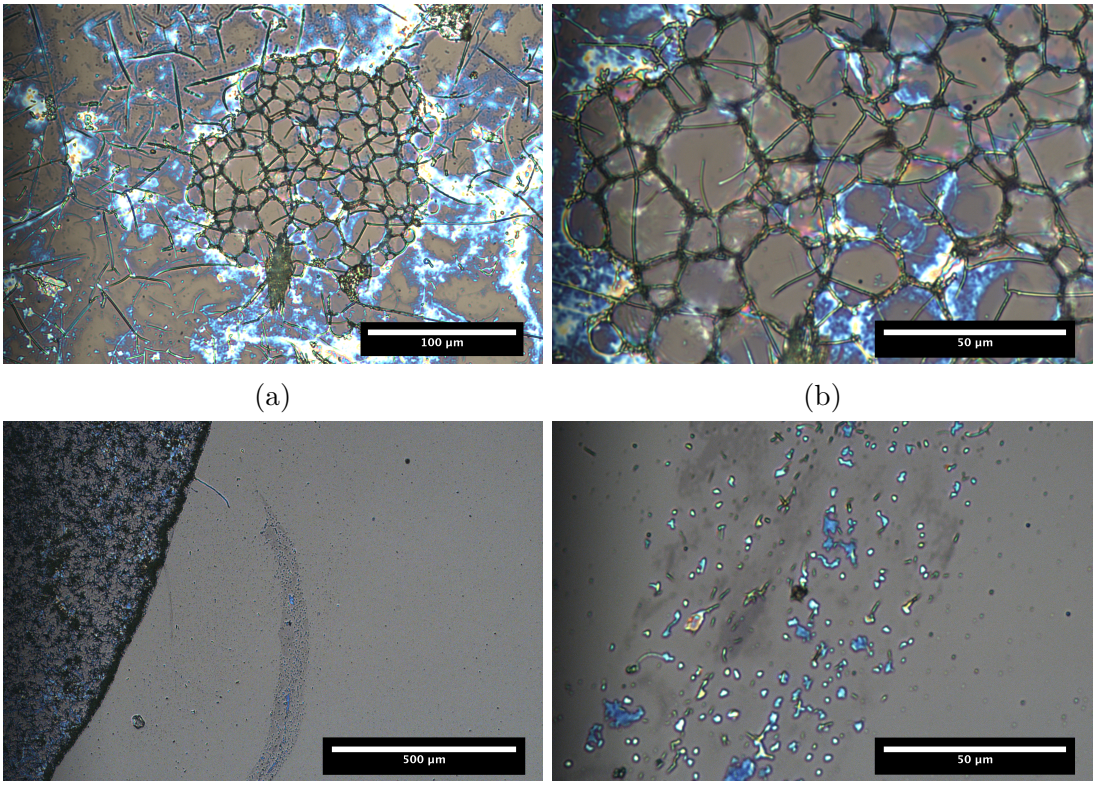

(a) (b)

(c) (d)

Figure 2.2: Two of the typical features of penetrating droplets: cell-like structures a)-b) and outer rings c)-d). Both were spotted only after the droplet evaporated fully. The cell-like structures were spotted always in the droplet centre. The outer rings always had elliptical shape and contained smaller particles than the average in the bulk droplet, as these could better fit in the channels made by the penetrating droplet.

2.2 The most dramatic case & proposed mechanism

In droplets shown in Fig. 2.1, we saw the riboflavin aggregates moving freely through the pockets and branches, flowing to form the coffee ring. From this we deduced that these features are somehow beneath the droplet, so they do not block the way for the aggregates. This was proven by observation of the pure water droplet shown in Fig. 2.3.

The droplet first showed spreading fractal branches (Fig. 2.3 (a) and (b)), which were also seen earlier, but then, suddenly, the droplet completely abandoned its spherical cap shape, assuming a crumpled shape with an irregular circumference (Fig. 2.3 (c) and (d)). There is no way a droplet in contact with air (or another fluid) would assume a shaped curved this much. It would instead seek to minimize the contact surface and smooth the undulations. Crumples like in Fig. 2.3 (c-f) are reminiscent of paper: indeed they can be produced by the deformation of a solid thin film. They could be formed if the droplet was somehow packed underneath the thin film.

This hypothesis is confirmed by a look at the surface left behind by the droplet in Fig. 2.4: revealing a cracked and bent thin film on a surface beneath it. Since the prolonged evaporation only happened on surfaces consisting of a Teflon thin film deposited onto an oxidized Si wafer, we conclude that the droplet must have somehow penetrated the Teflon layer and hid a part of its volume beneath it. Because this volume was hidden the droplet evaporated much slower.

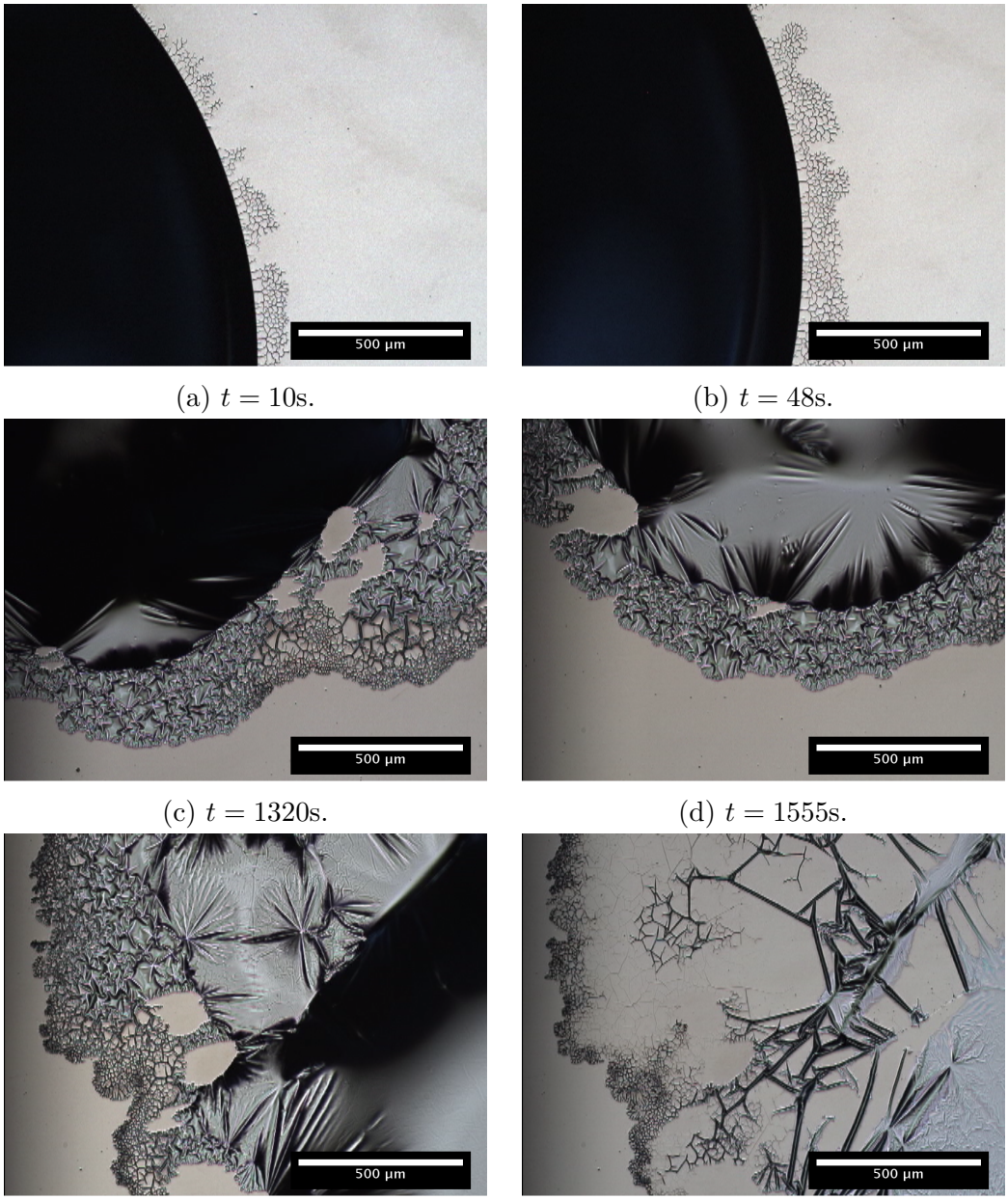

(a) $t = 10$s. (b) $t = 48$s.

(c) $t = 1320$s. (d) $t = 1555$s.

(e) $t = 1637$s (f) $t = 1962$s

Figure 2.3: Evaporation of a penetrating water droplet with initial volume 3μl on a PTFE/Si surface at 30°C. As the droplet permeates the surface, first branching arms formed and spread. Then, at a later time, the droplet lost its spherical shape as it permeated even further, forming rippling undulations. These further spread, and as the droplet evaporates, retracted. The state of the surface left behind by the droplet can be seen in Fig. 2.4.

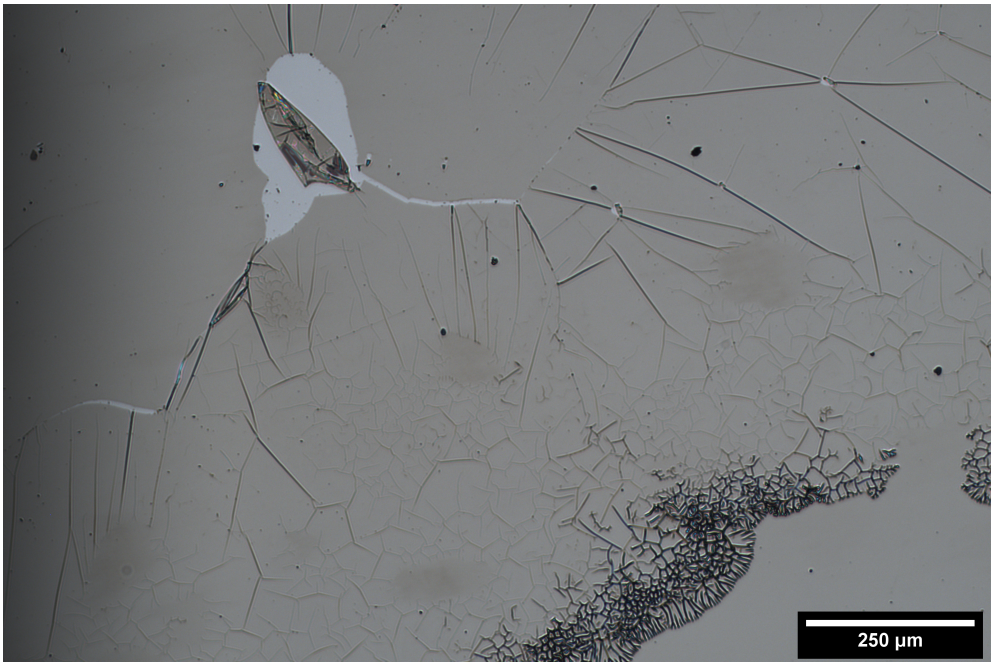

Figure 2.4: Photo of a PTFE/Si surface, after the water droplet from Fig. 2.4 evaporated on it. The Teflon layer is bent from the droplet's undulations and cracked, revealing the Si wafer beneath.

In the case of the water droplet in Fig. 2.3, almost all of the droplet hid under the layer and the droplet lost its spherical shape. In case of the riboflavin droplets in Fig. 2.1, a smaller part of them penetrated the layer and they retained the spherical shape, the hidden part instead forming the branches and pockets.

2.3 Solution: do not use old surfaces

Now that we knew that prolonged evaporation results from mechanical instability of the Teflon layer, we decided to use only Teflon surfaces that are at most one week old. On these surfaces, we have never seen droplets evaporating anomalously long or any of the typical penetration patterns from Fig. 2.1 and 2.2.

We have, however, managed to reproduce the patterns by letting a droplet evaporate on a heated surface. In Fig. 2.5 can be seen snapshots from a liposome-laden droplet (see Chap 3) for more details on a PTFE/Si surface that is heated to 50°C. It exhibits pockets reminiscent of Fig. 2.1. Due to the high temperature the droplet evaporated within 4min, so the prolonged lifetime was not seen.

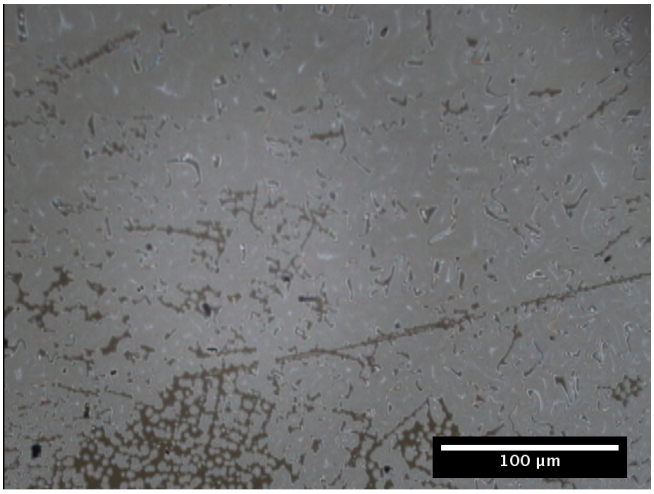

(a) $t = 127$s

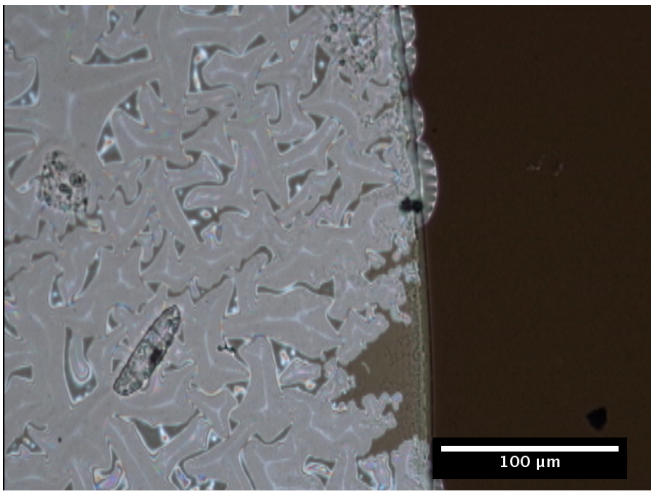

$t = 167$s

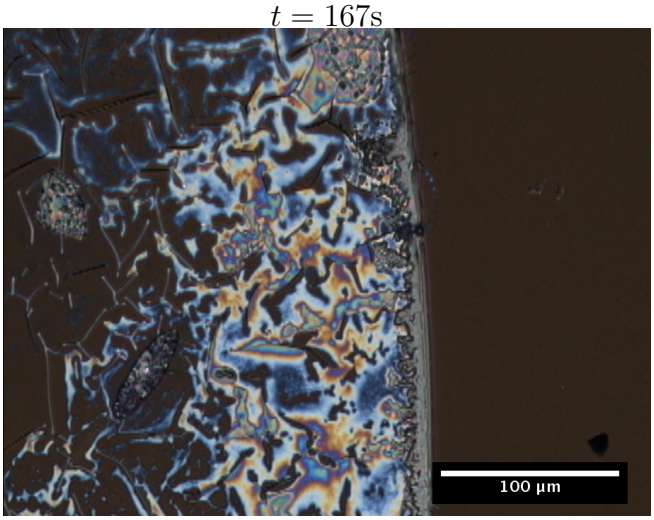

$t = 175$, dry.

Figure 2.5: A droplet of 0.5mg/ml DPPC suspension evaporating on a PTFE/Si surface at 50°C. Undulations and pockets can be seen in the images, indicating that the droplet now penetrates the surface layer, even though it was made within a week before evaporation. The high temperature makes the evaporation much faster, therefore the anomalous long evaporation time was not seen.

2.4 Theoretical analysis of the penetration

Why does the droplet penetrate the hydrophobic Teflon film, when in doing so it increases their mutual contact surface? We believe the answer lies below the Teflon film: in the SiO_2 layer. SiO_2 is polar and hydrophilic, and therefore its contact with Teflon is energetically unfavorable. By hiding under the film, the water in the droplet changes the phases it neighbors with: above the film it neighbors with the Teflon film and with air, beneath it neighbors with the film and with the SiO_2 layer.

Let us look at the energy balance of penetrating. When a part of the droplet hides beneath the layer, its contact area with the air shrinks by δS_{top}. Let us assume that this part forms a protrusion branch beneath, and that this branch will have contact area of δS_{bottom} with both the Teflon film and the oxide layer. Then, the energy difference resulting from penetration is:

$$\Delta E = -\gamma_{lg}\delta S_{top} + \delta S_{bottom}(\gamma_{lT} + \gamma_{lO} - \gamma_{TO}), \tag{2.1}$$

where γ_{lg} is the air/water surface tension, γ_{lT} the surface tension of the water/Teflon interface, γ_{lO} for the water/oxide and γ_{TO} teflon/oxide. For this process to be energetically favorable, the following inequality needs to hold:

$$\frac{\delta S_{top}}{\delta S_{bottom}} > \frac{\gamma_{lT} + \gamma_{lO} - \gamma_{TO}}{\gamma_{lg}}. \tag{2.2}$$

The respective γ values are material constants and the fraction $\delta S_{top}/\delta S_{bottom}$ depends on current droplet contact angle and radius and on the shape of the protrusions. This inequality therefore constrains the shape of the protrusion as a function of the droplet shape.

This consideration also yields a possible method to produce more stable Teflon surfaces and avoid penetration. The possible cause of the penetration is the unfavorable contact of the two materials forming the surface: of SiO_2 and Teflon, the first is polar and the second non-polar. If both materials were non-polar, they would stick together better (lessening γ_{TO}) and the water would not want to penetrate beneath the upper film, as it would not come to a favorable contact with a polar surface.

The solution to this is removing the SiO_2 layer: this way the Teflon film would be in contact directly with the non-polar Si bulk. The methods for removing the oxidation layer are discussed in [37], they include washing the surface either in an acid bath or in acetone. An alternative solution would be not letting the Si wafer to oxidize at all: cutting the Si to the wafers in the same vacuum chamber as the Teflon deposition is done.

3. Spreading of liposome-laden droplets: experiments

Raman spectroscopy is a versatile analytical method, capable of identifying chemicals in many different environments. A substantial disadvantage of this method is that the signal received is quite low, and high concentrations of the chemicals for detection are required. One of the ways the substance can be concentrated is by letting a droplet with the dilute solute evaporate and then detect the much more concentrated deposit [7].

This technique is developed at the Division of Biomolecular Physics in Institute of Physics at Charles University [6, 38, 39]. One of the molecules used for testing there are the liposome-forming lipids. In one of the experiments, droplets of liposome suspension started to gradually spread when evaporating. This is a novel phenomenon for evaporating droplets, as normally they either stay pinned or retract. We shall investigate this effect experimentally in this Chapter and theoretically in the next one.

3.1 Sample preparation

The lipid dipalmitoylphosphatidylcholine (DPPC) was used as a monomer to form the liposome vesicles. Its chemical structure can be seen in Fig. 3.1. It is an amphiphilic molecule, having a polar head and a non-polar tail. Because of this, in water DPPC can aggregate to micelles, bilayers and vesicles. A liposome is sketched in Fig. 3.2.

The DPPC suspensions used in this work were prepared at the Institute of Physics, Faculty of Mathematics and Physics, Charles University using the standard procedure from [40], described in detail in [41].

This resulted in a suspension of 100nm unilamellar DPPC liposomes with phase transition temperature at 41°C. We used concentrations ranging from 0.125mg/ml to 2mg/ml.

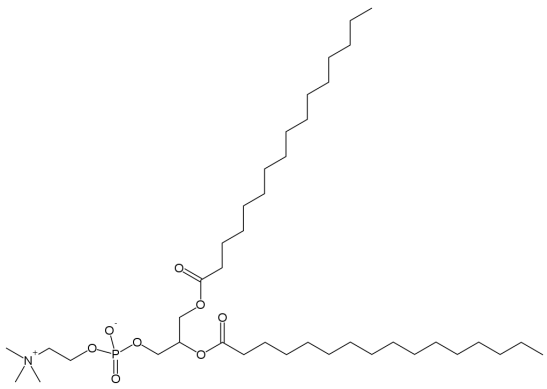

Figure 3.1: The chemical structure of dipalmitoylphosphatidylcholine (DPPC), showing the polar phosphatidylcholine head (left) and two nonpolar palmitoyl tails (right).

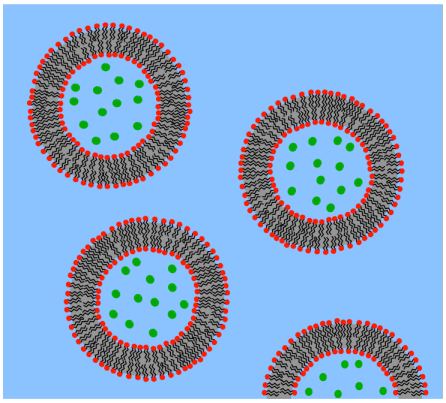

Figure 3.2: A schematic showing an unilammelar liposome composed of amphiphilic molecules in water. The molecules assemble into bilayers in which their polar heads (red) point to the water (blue) and their hydrophobic tails (black) touch each other. In this case, the bilayers form a spherical liposome, which can be used to store and transport cargo inside (green dots).

3.2 Surface preparation

We used two types of surfaces in our experiments: silicon wafers (SiO_2), and silicon wafers covered with a teflon plasma polymer (PTFE/Si). The first are made from crystalline Si and covered with a layer of SiO_2 created by oxidation. The second type is made from the wafer coated with plasma polymer by magnetron sputtering in an argon atmosphere with pressure 19Pa (for specifics, see [15]). This process creates a smooth hydrophobic layer. The contact angle of water on the SiO_2 surfaces was $40 - 45°$, for PTFE/Si it was $105 - 110°$. Surfaces used in experiments in Chapter 2 were up to one year old, surfaces used in experiments in Chapter 3 were no older than one week.

3.3 Light microscopy

To gain a qualitative understanding of the detailed processes inside the evaporating droplet, we observed the evaporation with bright-field microscopy. As a microscope we used *Nikon Eclipse 80i* upright microscope with Epi-fluorescence attachment, though we only used the bright-field mode. The microscope is equipped with Flyeye illumination system containing a 100W halogen lamp. It is furnished with four different objectives: *Nikon LU Plan Fluor* 5×, *Nikon LU Plan Fluor* 10×, *Nikon LU Plan* 20× and *Nikon LU Plan* 50×, which could be interchanged manually. The data were collected using DFK33UX178 USB camera and processed either into an image or a video using the software *IC Measure*. The microscope sample holder is placed in a temperature control unit which we used to record the evaporation process at a given constant temperature. The sample holder is movable and has a slot of a size of a glass slide. Therefore, to be able to move the surface with the droplet while recording, the surface was put onto a glass slide which was inserted into the slot in the holder. Because the surfaces used do not transmit light, only the reflection mode of the bright-field microscopy was used.

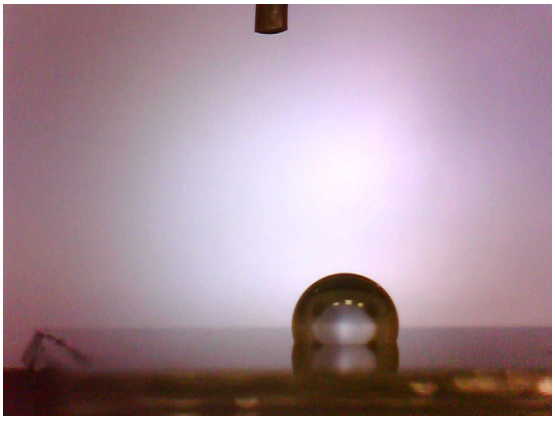

Figure 3.3: Sample image of an evaporating droplet acquired in our laboratory, dropped from a syringe onto a silicon wafer.

3.4 Measuring droplet shape dynamics

Droplets with DPPC suspensions of chosen concentrations ($0.125-2$mg/ml) were dropped on either PTFE/Si or SiO_2 surfaces under $20-23\%$ humidity and ambient temperature $23-27$°C, both of which we could not control. We could control the temperature of the surface, which we, unless otherwise stated, fixed at 30°C. The volume of the droplets was either 2 or 4μl and they were dropped from a micropippete held by hand. The evolution of the droplet was recorded using an apparatus constructed at the Department of Macromolecular Physics, consisting of a camera, LED illumination shielded by a rough plexiglass to diffuse the incoming light, and pedestal calibrated with a spirit level to ensure horizontal alignment. In practice, a small tilt in the direction of the camera was used to allow also the reflection of the droplet to be seen. The images from the camera were captured using the software *Webcam Frame Capture* [42], one every second. Sample image acquired by the camera is in Fig. 3.3.

3.5 Image processing

The sequence of images taken from the whole evaporation of a droplet was converted to grayscale and cropped so that only the area around the droplet was kept. Usually only every fifth image was imported, but for rapid changes a finer period was chosen. Droplet shape was analyzed using DropSnake (see Chapter 1) with the script included in the Attachments, which allowed for automatic processing of the whole droplet evolution sequence.

The images we acquired have one disadvantage the fitting algorithm cannot properly deal with: the tilt of the surface. The precise orientation of the surface could be controlled and could be made horizontal, but we chose to tilt it a little toward the camera. This allows the reflection of the droplet to be seen in the camera (as in Fig. 3.3), allowing for better droplet shape fitting. When the contact angle is large, the tilting does not alter the image significantly. For small contact angles, however, a tilted image looks like it has a higher contact angle, and a higher radius, see Fig. 3.4. This had to be taken into consideration when interpreting the data.

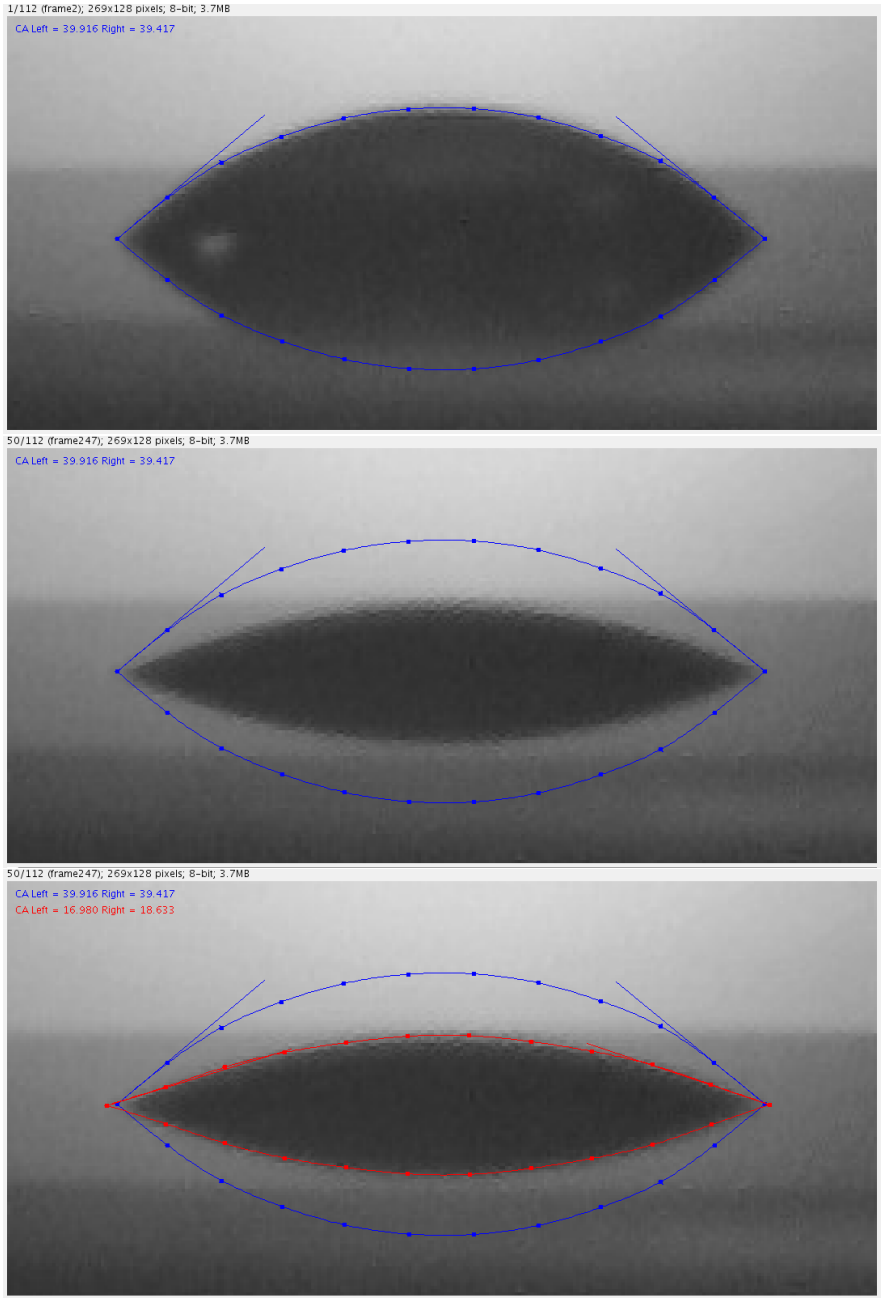

Figure 3.4: Example of the fake droplet spreading resulting from the surface and the droplet being tilted, which the fitting algorithm recognizes as higher contact angle and greater radius. The top image shows a droplet at evaporation time $t = 12$s with $\theta = 30°$, the blue lines a fit by DropSnake. The algorithm fits the shape correctly. The middle shows a frame from the same droplet later at $t = 257$. It can be seen that the droplet now has a smaller θ, but still the same radius as on the frame before. In the bottom image DropSnake fits the current droplet shape (red curve). Because of the tilt, the fitting yields a larger radius than the blue curve did, resulting in the fake spreading.

3.6 Results

3.6.1 Drop shape dynamics

The results of the image analysis for the droplets evaporating on PTFE/Si surface are in Fig. 3.5, 3.6, 3.7 and 3.8 and for droplets evaporating on SiO_2 in Fig. 3.9. Pure water droplets in Fig. 3.5 show typical droplet shape dynamics with both CCR and CCA modes, the receding contact angle being about 66.5°. These droplets are not influenced by any solute within and therefore serve as a reference sample for the liposome suspension droplets.

The basic difference that all the DPPC droplets exhibit is the lack of the receding phase, i.e., the hysteresis of the contact angles becomes so large that θ_R becomes lesser than 0° and the contact line becomes pinned. This is a feature common in all suspension droplets, as the coffee ring that is created in the evaporation process acts as a powerful droplet-wide defect that can prevent receding at all.

The second striking feature in the liposome-laden droplets is that some of them spread, namely droplet in Fig. 3.6 (blue), in Fig. 3.7 (blue) and droplets in Fig. 3.8 (blue, green, orange). Observed magnitudes of this effect range from 5% to 25%. The microscopic mechanism of this effect is discussed in Chapter 4.

For droplets Fig. 3.6 (blue), in Fig. 3.7 (blue) and droplets in Fig. 3.8 (blue), there is a period of constant radius followed by spreading, whereas droplets in Fig. 3.8 (orange, green) spread from the very beginning. In all the spreading droplets there is at least one re-pinned phase where the droplet ceases to spread. Sometimes (in droplets Fig. 3.6 (blue), Fig. 3.8 (orange, green)), after this pinned phase, another spreading phase occurs. We believe this to be simply caused by the observed part of the droplet being locally pinned by a stronger defect. If the drive of the droplet to spread is still strong enough, it can overcome the defect and spread further.

Droplets in Fig. 3.8 (blue) and perhaps also in Fig. 3.9 (red) exhibit spreading in the first 20s of the evaporation process. Spreading at these times is the result of quick relaxation processes on the surface that do not involve any evaporation, adsorption or flows, and which we here simply call *relaxation*.

In many cases the droplet radius calculated by the image analysis algorithm rises rapidly in the last part of the evaporation process. This is likely caused by the small-angle/tilt interference described above in Sec 3.5.

In Fig. 3.5, we can see that the total evaporation rate is approximately constant while the contact line is pinned and gradually decreases when the droplet evaporates, in agreement with the results from [30] described in Chapter 1.

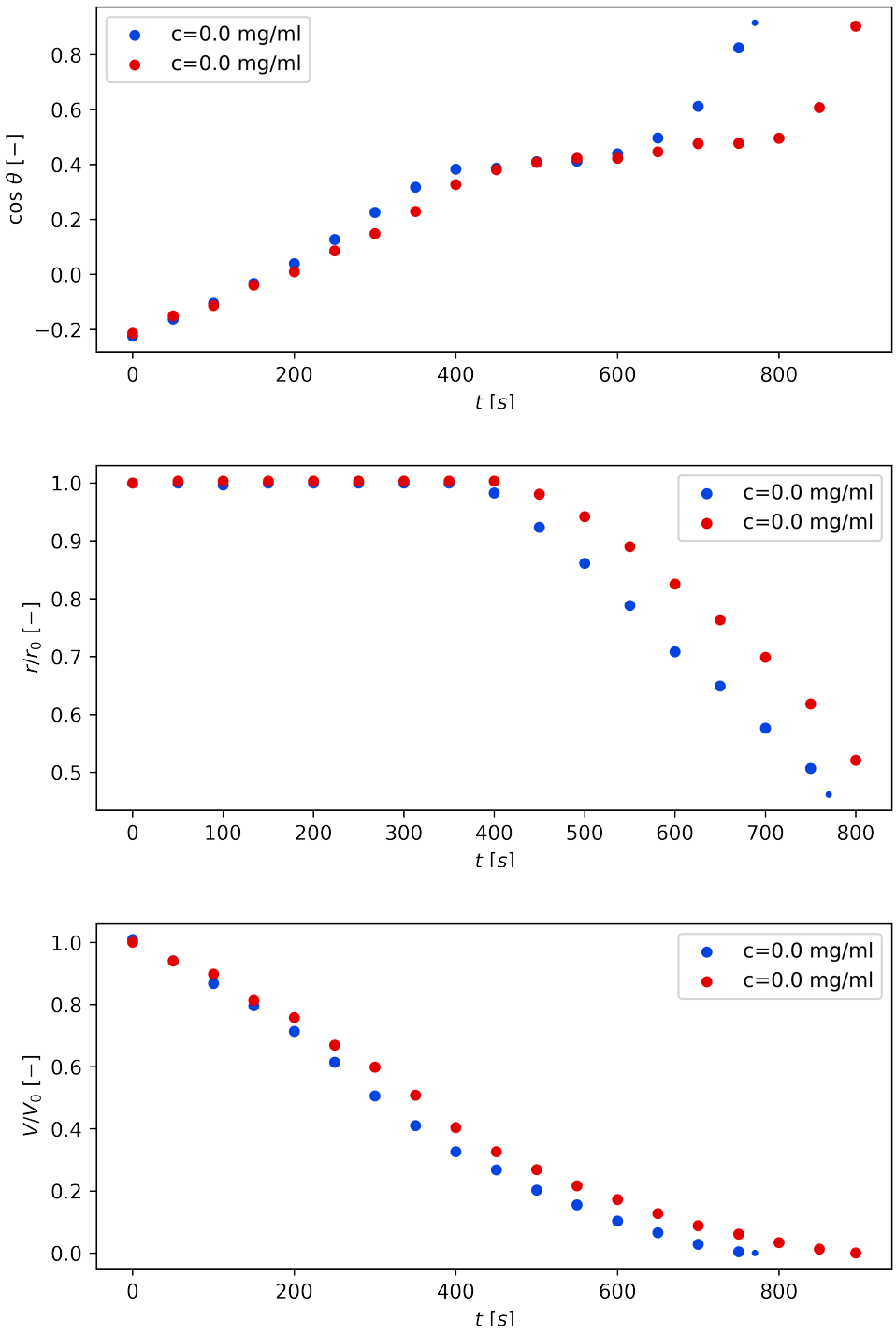

Figure 3.5: Evaporation dynamics of two 2μl droplets of pure water, evaporating on PTFE/Si surface. Evolution of radius (middle) and cosine of the contact angle (top) showing the CCR, CCA and MM phases. Volume evolution (down) showing a change in evaporation rate resulting from the transition from CCR to CCA mode. Data with $\theta < 25°$, where the fitting algorithm stops being accurate, are plotted with smaller markers.

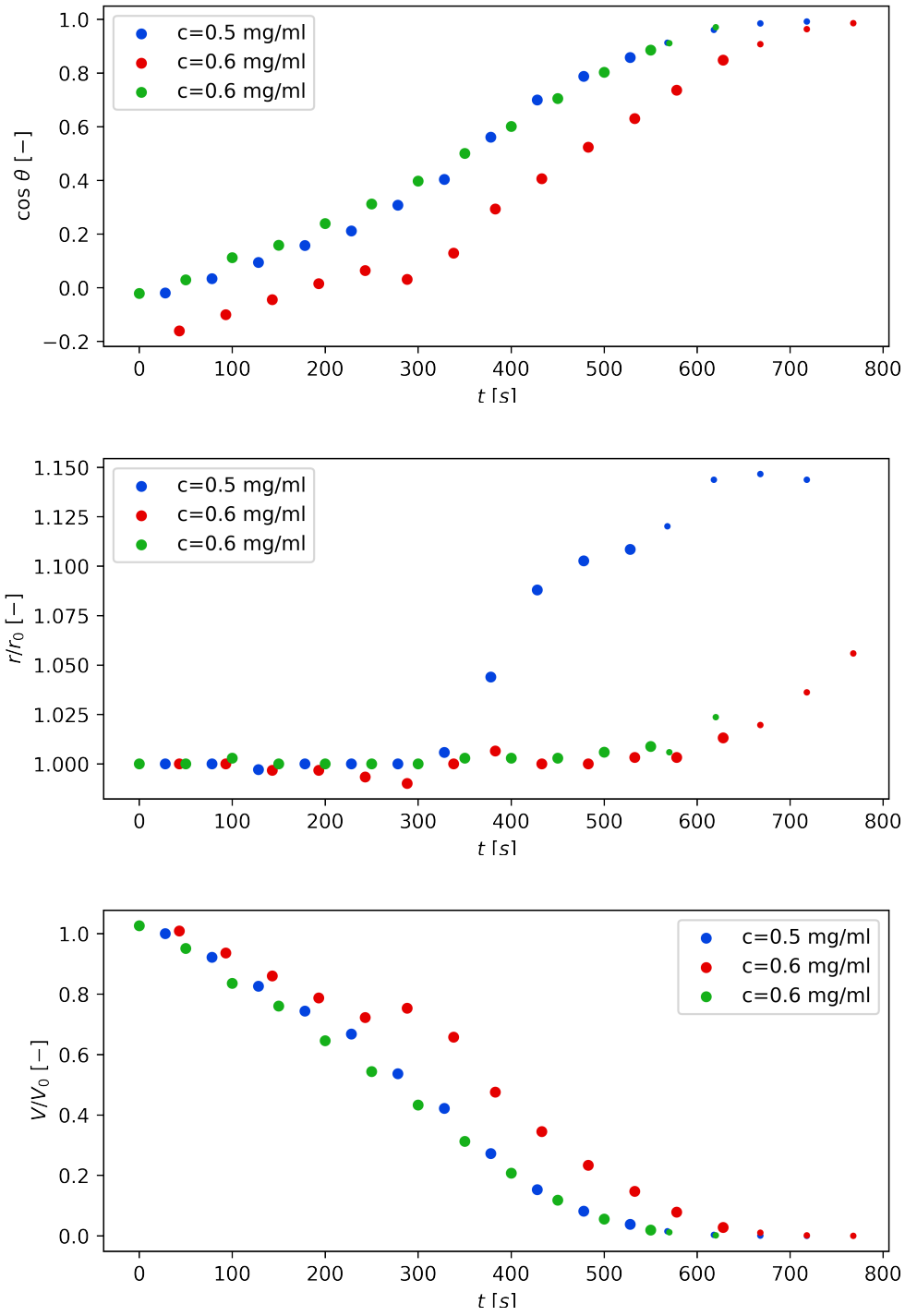

Figure 3.6: Evaporation dynamics of 2μl DPPC suspension droplets with initial concentrations $c = 0.6$mg/ml (red and green) and 0.5mg/ml (blue), evaporating on PTFE/Si surface. Evolution of radius (middle) and cosine of the contact angle (top) showing a pinned contact line for both 0.6mg/ml droplets and spreading for the 0.5mg/ml droplet. Volume evolution (bottom) showing almost linear volume decrease for the pinned droplets and a weakly nonlinear one for the spreading one, in both cases transitioning to a late-time power-law decrease. Data with $\theta < 25°$, where the fitting algorithm stops being accurate, are plotted with smaller markers. The late-time ($t > 550$s) spreading for the two $c = 0.6$mg/ml droplets is likely a numerical artefact.

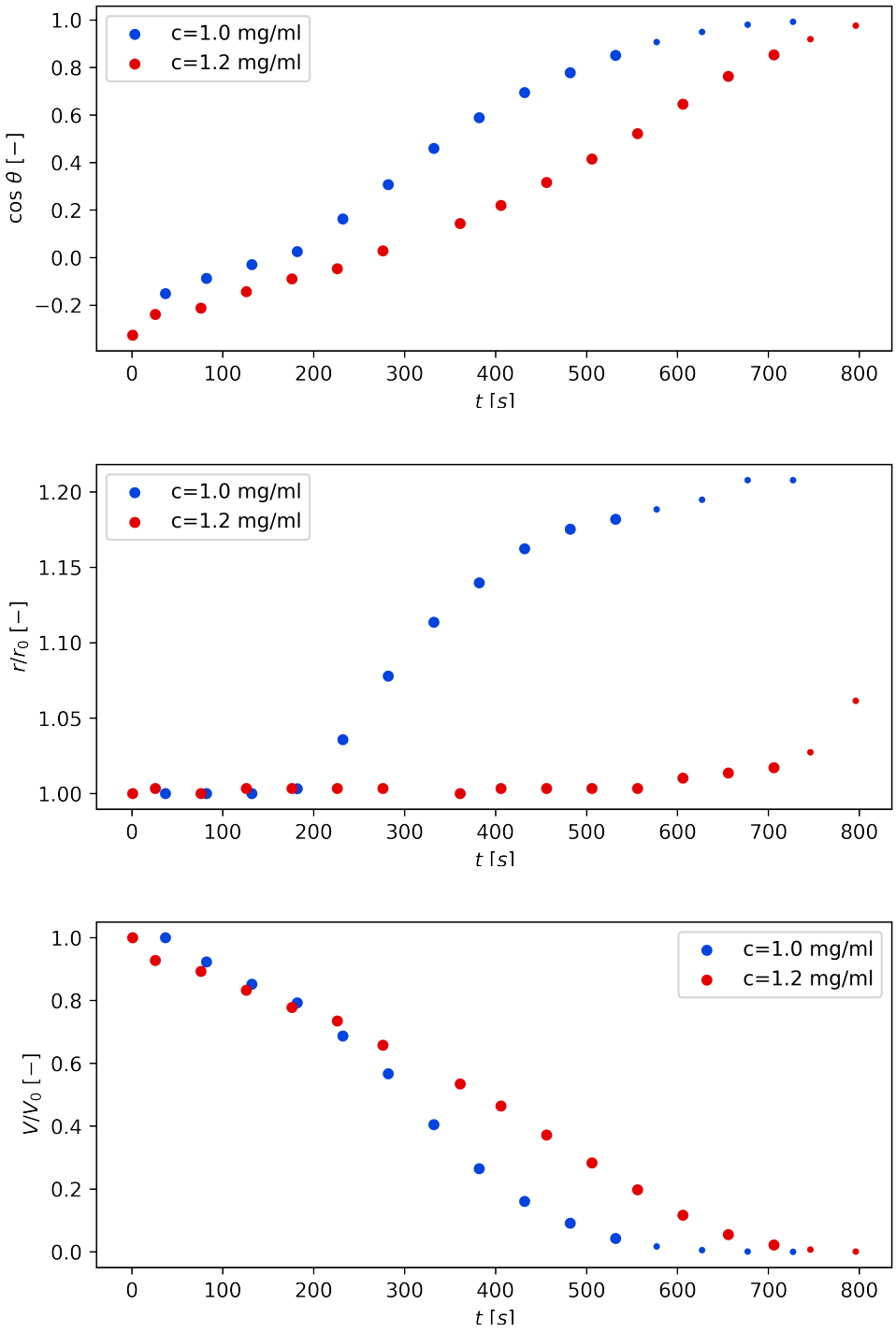

Figure 3.7: Evaporation dynamics of 2μl DPPC suspension droplets with initial concentrations c = 1.0mg/ml (blue) and 1.2mg/ml (red), evaporating on PTFE/Si surface. Evolution of radius (middle) and cosine of the contact angle (top) showing a pinned contact line for the 1.2mg/ml droplet with perhaps a slight spreading after 500s and significant spreading with a sudden start for the 1.0mg/ml droplet. Volume evolution (down) showing almost linear volume decrease for the pinned droplet and a nonlinear one for the spreading one, in both cases transitioning to a late-time power-law decrease. Data with $\theta < 25°$, where the fitting algorithm stops being accurate, are plotted with smaller markers. The late-time spreading ($t > 750$s) for the $c = 1.2$mg/ml droplet is a numerical artefact.

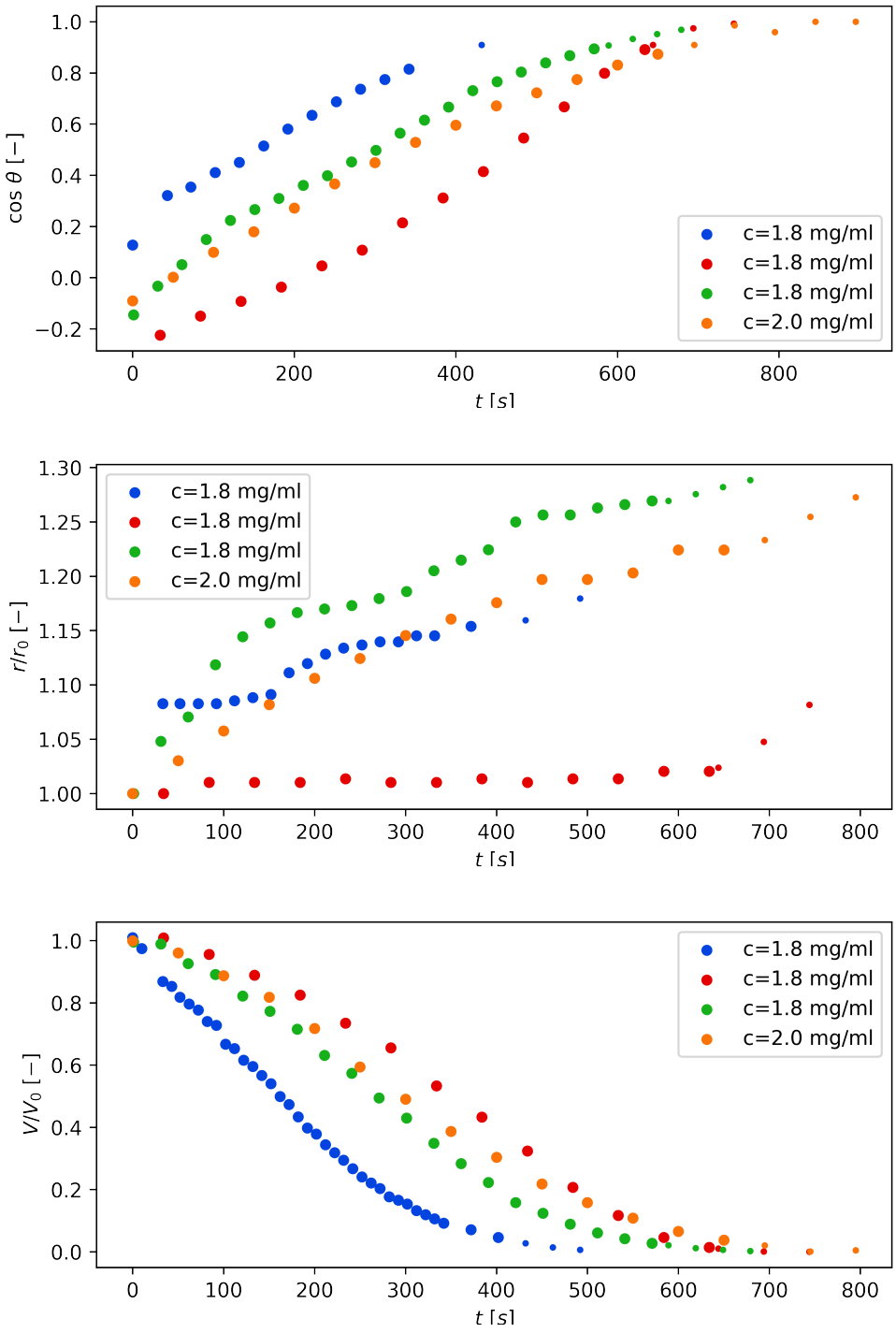

Figure 3.8: Evaporation dynamics of 2μl DPPC suspension droplets with initial concentrations $c = 1.8$mg/ml (red, blue, green) and 2.0mg/ml (orange), evaporating on a PTFE/Si surface. Evolution of radius (middle) and cosine of the contact angle (top) showing either pinning or spreading. The blue and red droplets show an early spreading followed by a pinned contact line followed by abrupt spreading at 180s (blue) and probably a false late spreading (red). The green and orange droplets spread from the very beginning steadily until around 420s. The orange droplet then spreads again at around 580s. Data with $\theta < 25°$, where the fitting algorithm stops being accurate, are plotted with smaller markers. Spreading for these values is a numerical artifact.

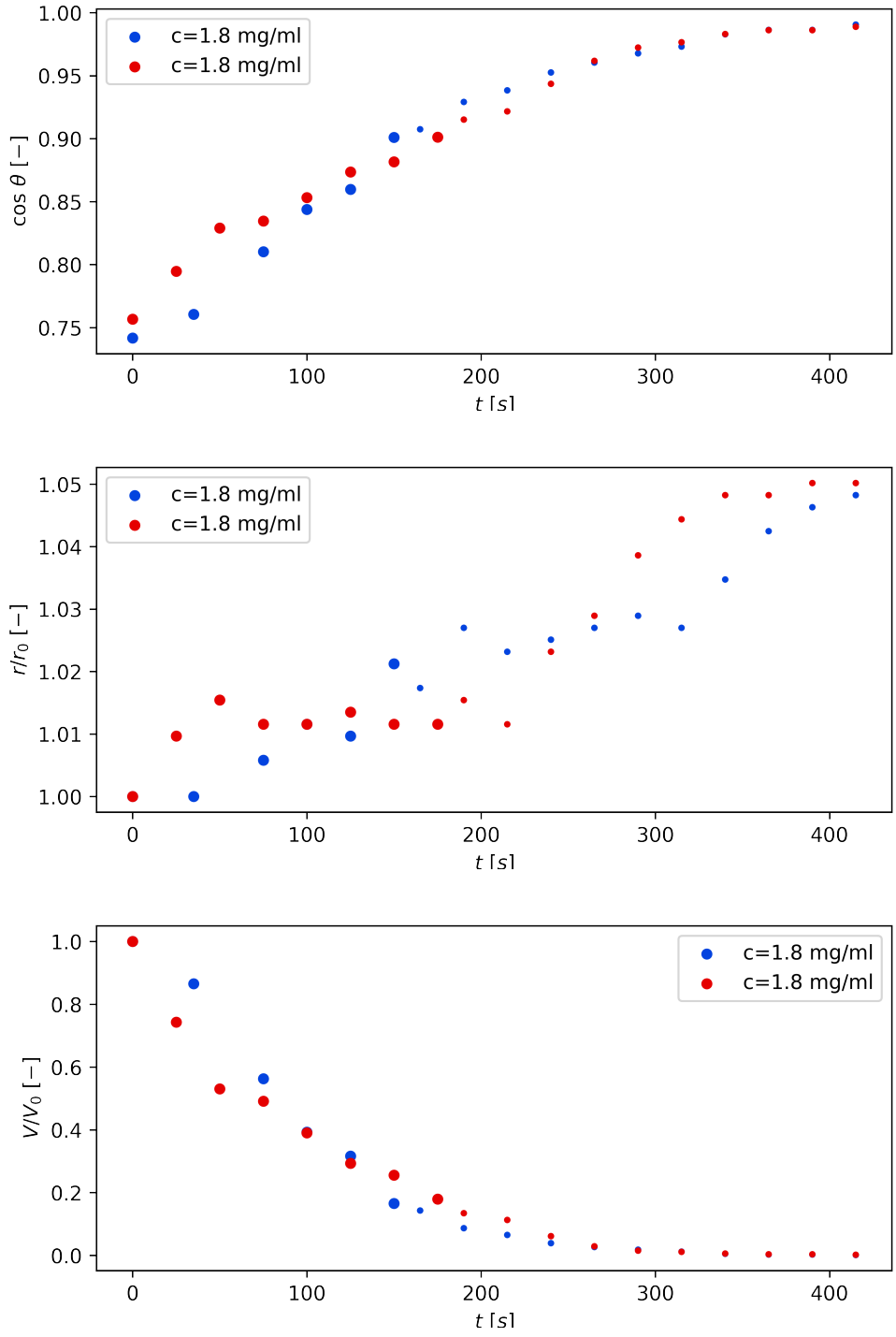

Figure 3.9: Evaporation dynamics of 2μl liposome suspension droplet with concentration $c = 1.8$mg/ml, evaporating on a surface of silicon. Evolution of radius (middle) showing spreading at late times which is likely a numerical artefact, as on SiO_2 already the starting angle (top) is quite small. Volume evolution (bottom) showing an weakly nonlinear volume decrease transitioning to a late-time power-law decrease.

3.6.2 Effect of DPPC on surface tension

We have measured the initial contact angle of liposome-laden droplets for varying DPPC concentrations. The results can be seen in Fig. 3.10: the initial contact angle is not significantly affected by changing the concentration.

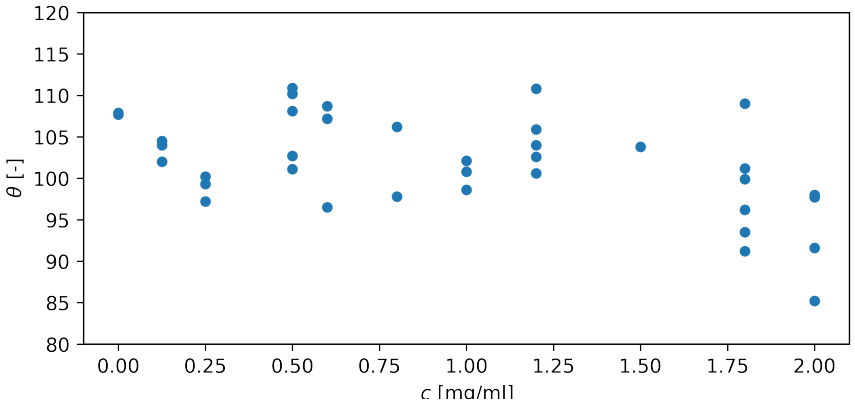

Figure 3.10: Initial contact angle θ for droplets of different DPPC concentrations. For a given concentration, the values differ due to contact angle hysteresis and the inaccuracy of the dropping due to human factor. This hysteresis is greater than any effect the liposomes have.

4. Spreading of liposome-laden droplets: interpretation of results

The fact that DPPC-laden droplets spread was observed by González-Gutiérrez et al. in [22]. The authors studied the morphology of the deposits left behind by the droplets and found that deposit diameter exceeded the evaporation temperature was increased above the phase transition temperature of the liposomes T_m, which for DPPC liposomes is 41°C. The results are shown in Fig. 4.1. They also performed light microscopy measurements of the evaporation, see Fig. 4.2, where saw the droplets spread at the beginning, but only above T_m. We have, in our experiments (with a different hydrophobic surface than in [22]), observed this spreading also below T_m. González-Gutiérrez et al. attribute the spreading to the fluid-like nature of the the vesicle bilayers, which is not valid if the phenomenon happens also below T_m. We set out to find a robust explanation of this spreading.

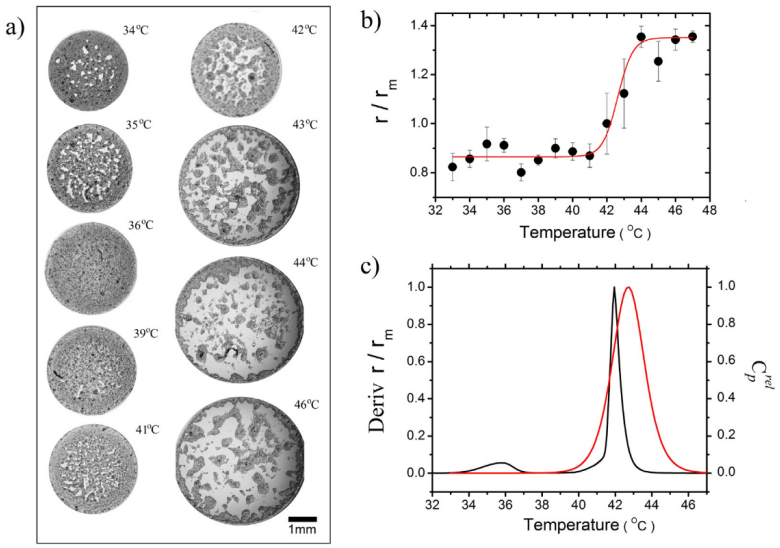

Figure 4.1: Temperature dependence of the morphology and diameter of deposits made by evaporating DPPC laden droplets. a) Overview of the deposits for the different temperatures. The diameter grows with temperature and the morphology changes from almost homogenous to inhomogenous. b) The radius r changes in a sigmoid fashion as the evaporation temperature exceeds the phase transition temperature of the liposomes. c) Correlation of $\partial r/\partial T$ and the calorimetric data. Adapted with permission from [22]. Copyright 2017 Elsevier.

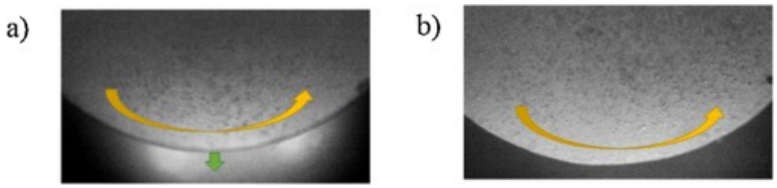

Figure 4.2: Snapshots of an evaporating DPPC-laden droplet, showing spreading. The yellow arrow shows the circulatory Marangoni flow, the green arrow the spreading direction. Adapted with permission from [22]. Copyright 2017 Elsevier.

4.1 Review of literature

Since the liposomes are made of surfactant molecules, it is to be expected that they modify surface tensions in the droplet. There are two interfaces on which they can act: the air/water interface and the water/surface interface. While works studying liposomes directly in evaporating sessile droplets are lacking, there are plenty of works where the effect on one of these interfaces was studied.

4.1.1 Adsorption of liposomes on air/water interface

In [16], the authors measured the time dependence of γ_{gl} using *bubble methods* [43], where the surface tension is obtained by measuring the induced pressure on an air bubble in the liquid of interest. The bubble can either pulsate periodically or be static.

They found that the tension γ_{gl} of DPPC disperions changes with time in a sigmoid fashion with a characteristic time $t_0 = 10^3 - 10^4$s. This time depends on liposome size and the way they were prepared. The authors measured zero solubility of the DPPC monomers in water, and therefore there cannot be an equilibrium of the monomers escaping liposomes and binding to the water/air interface.

Instead, the authors hypothesize that the liposomes stay intact until they diffuse to the surface, where they open up, see Fig. 4.3. Upon disintegration, they form an insoluble lipid layer that reduces the surface tension. This unwrapping takes time, and the liposome concentrate near the surface.

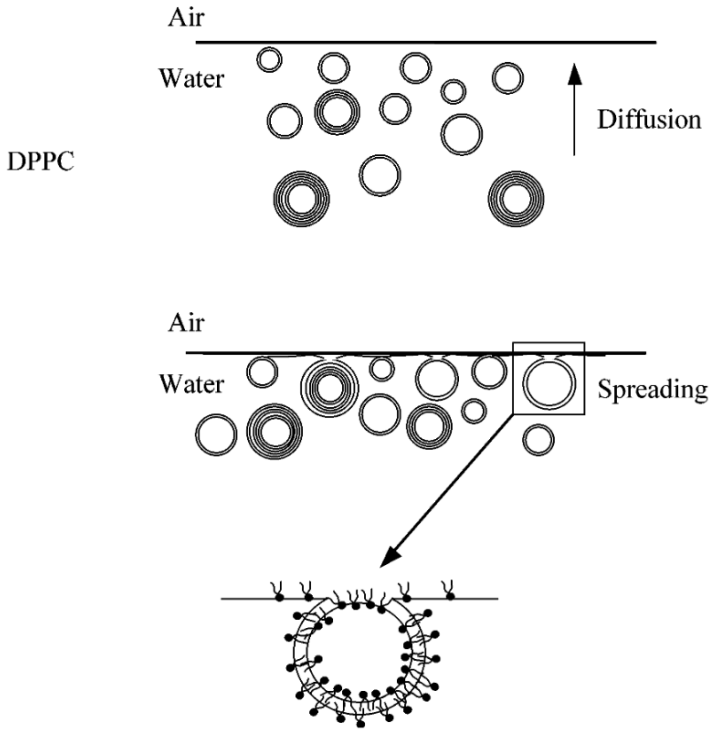

Figure 4.3: Hypothesized pathway for adsorption of DPPC on the air/water interface. The vesicles first diffuse near the interface and then bind and unwrap on it, forming a single lipid layer. Adapted with permission from [17]. Copyright 2002 American Chemical Society.

This has been reinforced by simulations in [44], where the authors used coarse-grained molecular dynamics to simulate the adsorption of a DPPC liposome. They saw that when the liposome came into contact with the air/water interface, the outer lipid layer of the bilayer liposome unwrapped and formed a layer at the interface of the two phases, see Fig. 4.4 a). The formation of this layer resulted in a surface tension drop. The inner lipid layer, however, did not unwrap, and ended forming an inverted micelle on the air side of the interface. The authors suppose these can travel along the surface and merge. The simulations show the micelles inducing local curvature on the surfactant layer at the interface, contributing to surface tension. The resulting surface tension was about $\gamma \approx 55\text{mN/m}$, which is a considerable drop from the standard 70mN/m for water.

Bai et al. [44] also performed similar simulation, shown here in Fig. 4.4 b), with the liposome approaching an interface between water and a hydrophobic substrate. Here the outer lipid layer also unwrapped and an inverted micelle remained from the inner lipid layer. Now, however, the interface could not be locally curved by the micelle, which caused the micelle to eventualy puncture and spill into the water phase. Also, the formation of the interface layer was faster in this case than on the air/water interface.

Bai et al. [44] also performed experiments with DPPC liposome suspensions, where they measured γ_{gl} by *constrained drop surfactometry* [45]. They did three different types of experiments. In the first type, liposome suspension was injected inside a droplet of pure water. In the second type, this suspension was spread directly onto the droplet surface. In both of these experiments, the equilibrium value of surface tension reached was the same, $\approx 40\text{mN/m}$. They did, however, differ in the relaxation timescale. For type 2 it was around 100 seconds, whereas for type 1 around 1000s, noting at the considerable time it takes to transport the liposomes to the vicinity of the interface. In the third type, the suspension of DPPC was dissolved in chloroform so it did not form liposomes and then spread onto the droplet surface. This type quickly reached an equilibrium value of $\approx 20\text{mN/m}$. Bai et al. attribute the difference in the equilibrium tensions to the presence of the inverted micelles in type 1 and 2 which contribute to surface tension.

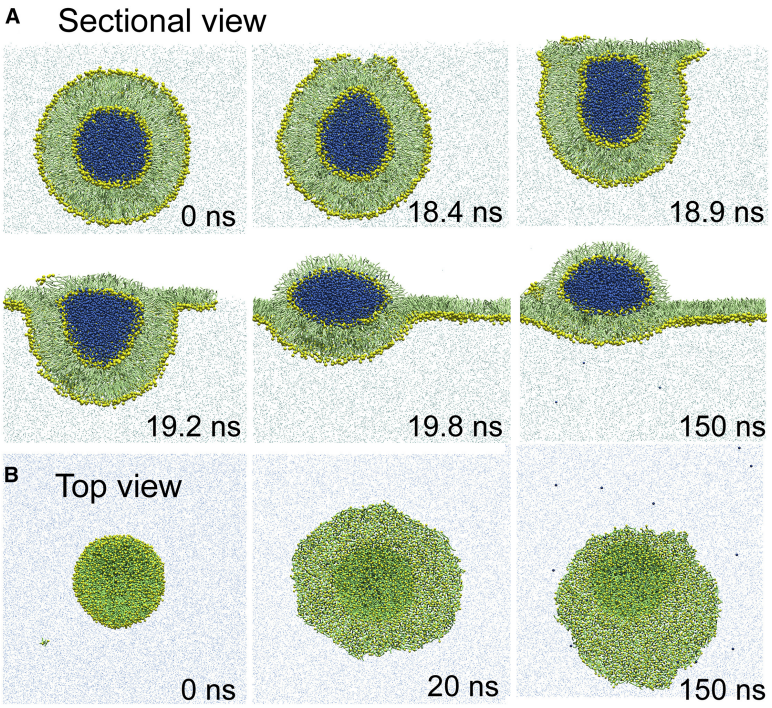

(a)

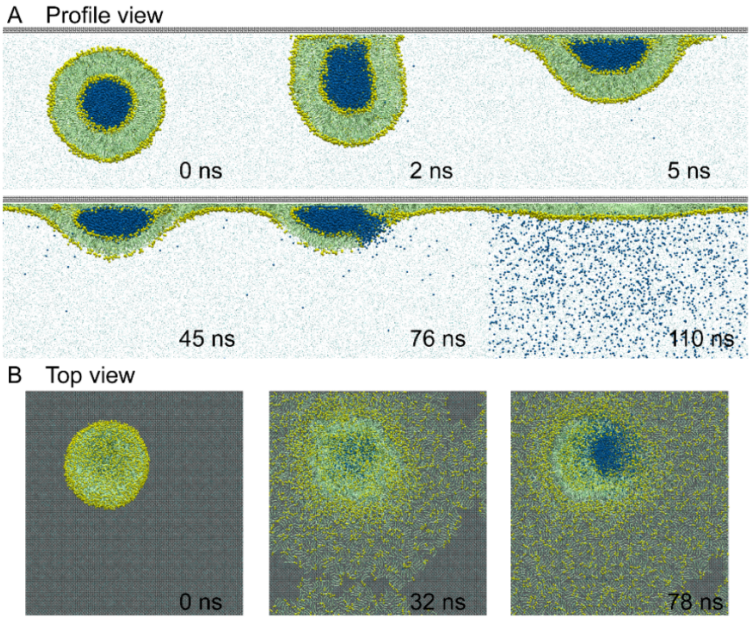

(b)

Figure 4.4: Snapshots from a coarse grained molecular dynamics simulation of a lipid vesicle adsorbing on the air/water interface (above) and on a hydrophobic surface (below). Color code: water- blue lipid polar head- dark green, lipid nonpolar tail-light green. In the air/water case the vesicle adsorbs on the surface, and the outer lipid layer unwraps, the inner staying in an inverted micelle facing the air phase. Supposedly, these micelles can diffuse on the interface and merge. In the water/surface case, the vesicle adsorbs on the surface, and the outer lipid layer unwraps, the inner stays in an inverted micelle facing the surface, which then ruptures, spilling to the outside. What remains is a lipid monolayer adsorbed on the hydrophobic surface. Adapted with permission from [44]. Copyright 2019 Elsevier.

4.1.2 Adsorption of lipid vesicles on surfaces

DPPC liposomes in our dispersions can adsorb also to the second interface the droplet: the water/solid interface. The adsorption mechanism is different for hydrophilic and hydrophobic surfaces, so we shall cover them separately.

Hydrophilic surfaces

Adsorption to hydrophilic surfaces (mostly to SiO_2, as is our case) has been widely studied [18, 46, 47], as it leads to formation of lipid bilayers, useful as a model to biological membranes for synthetic biology [48] or in nanotechnology [49]. The most of the works report that for electrically neutral vesicles, such as DPPC, there are two different pathways from an adsorbed vesicle into a bilayer, based on whether they are in gel or fluid state (above or below liposome transition temperature T_m)[18].

For neutral vesicles with membranes in the gel state, vesicles are adsorbed individually and stick to the surface, until a critial contentration Θ_c is reached. Then they merge into a single bilayer [46], called *supported bilayer* [50], see Fig. 4.5. Above T_m, the merging of vesicles into bilayers happens for all concentrations of adsorbed vesicles, which results in many disconnected bilayer sites [18] for low concentrations.

A more recent work [51], where the effect of vesicle size for specifically DPPC liposomes was investigated, reports that liposomes larger than 150nm stay intact when adsorbed on the surface, but 90nm large liposomes merge into a bilayer structure. Ref. [47] reports also intact adsorbed vesicles for 400nm large DPPC liposomes at 25°C.

All these experiments were conducted in a liquid with no flow and no temperature gradients. Also, the concentration Θ_c was reported to depend on temperature, vesicle size and type of buffer used [18]. It is therefore questionable how applicable are the findings to a system of an evaporating liposome-laden droplet. However, in our opinion, the qualitative findings (formation of the supported bilayer and intact adsorbed vesicle states) are also feasible in our experimental setup.

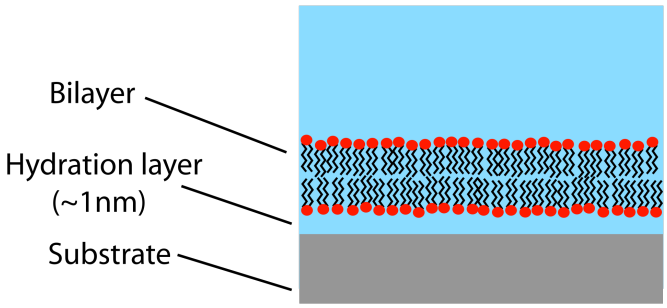

Figure 4.5: A sketch of a supported lipid bilayer floating above a hydrophilic surface. The individual lipid molecules are attracted to the surface and do not diffuse within the leaf as in free bilayers or cell membranes. Image adapted from [52].

Hydrophobic surfaces

The adsorption of lipid vesicles on hydrophobic surfaces is less explored, as it does not easily produce such well defined useful structures as on hydrophilic surfaces. Ref. [53] reports adsorption of single vesicles to the surface followed by vesicle rupture and unzipping into a single layer, as drawn in Fig. 4.6.

In [54], however, the authors used Quartz Crystal Microbalance (QCM) to study the adsorption process. QCM detects adsorption to a quartz crystal surface by measuring the frequency of acoustic waves of the crystal. For the hydrophobic surface the authors of [54] used, they did not detect any transition of adsorbed vesicles, merely simple first-order kinetics formation of a monolayer.

Rather interesting is a study [55] employing coarse-grained molecular dynamics. It reports two possible vesicle adsorption pathways for hydrophobic surfaces, depending on whether the surface is oleophilic or oleophobic. For oleophilic surfaces, the pathway is as [53] suggested, shown in Fig. 4.7. For oleophobic surfaces, depicted in Fig. 4.8, the mechanism is remarkable: no layer spreads on the surface, instead the vesicle unwraps onto the surface, forming a stable thimble-like structure, where the lipid molecules in contact with the surface are oriented parallel to it. In the study, however, only a single isolated vesicle was simulated. It is therefore unclear how the this mechanism would be altered by the mutual presence of many vesicles.

Yet another interesting mechanism has been proposed in Ref. [56], where the authors investigated an adsorption of a micrometre-large giant unilamellar vesicle with fluorescence microscopy. The authors state that the vesicles, upon adsorption, unwrapped into a dangling bilayer-like structure that then unzipped into a single layer on the hydrophobic surface. We consider this behaviour highly unlikely to happen in our case of smaller vesicles, because of the large curvatures in them that would make this kind of unzipping very hard.

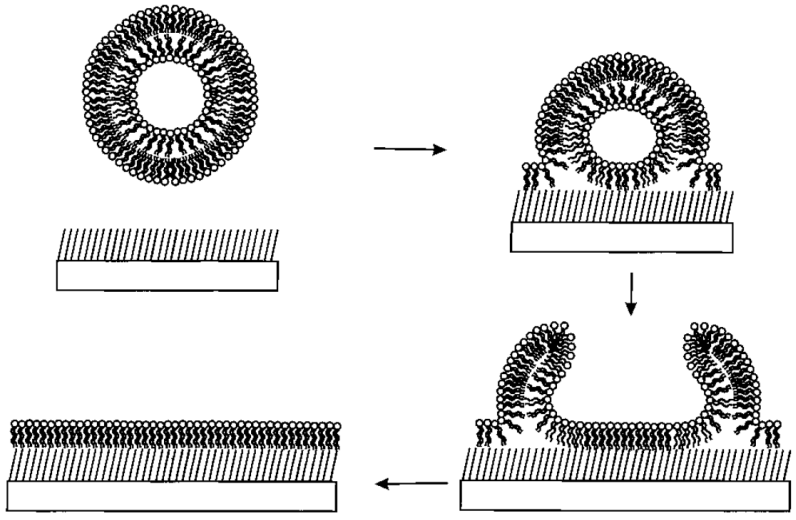

Figure 4.6: Hypothesized pathway for the adsorption of vesicles on a hydrophobic surface. The vesicles first diffuse near the interface, bind to it with the outer layer of their bilayer. Then the vesicle ruptures, spilling its contents and unzips on the surface, as a bilayer would, forming a lipid monolayer. Adapted with permission from [53]. Copyright 1997 American Chemical Society.

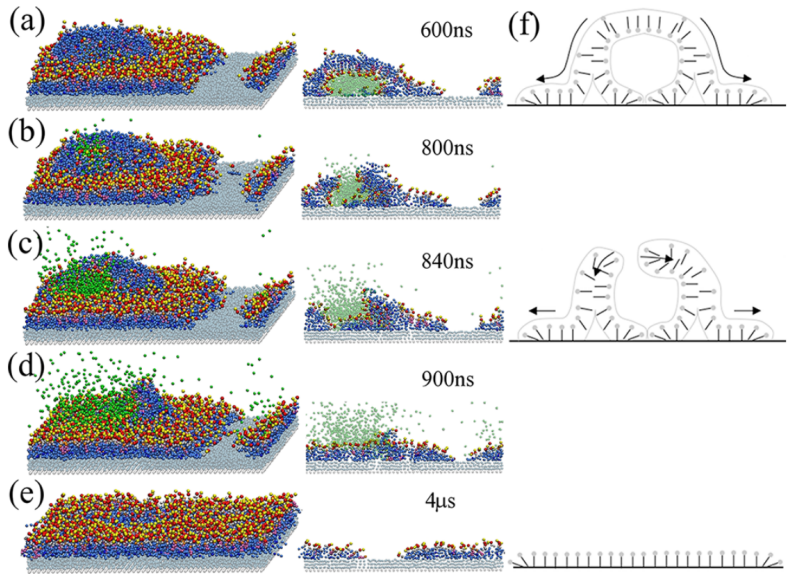

Figure 4.7: Snapshots from a coarse grained molecular dynamics simulation of a lipid vesicle adsorbing on a hydrophobic, oleophilic surface. Left column view from outside, middle column view on the vesicle perpendicular to the surface, right column cartoon showing the rupture. Color code: water-green, lipid polar head- red and yellow, lipid nonpolar tail-blue. The vesicle adsorbs on the surface, then ruptures and unzips, forming a lipid monolayer. Adapted with permission from [55]. Copyright 2002 American Chemical Society.

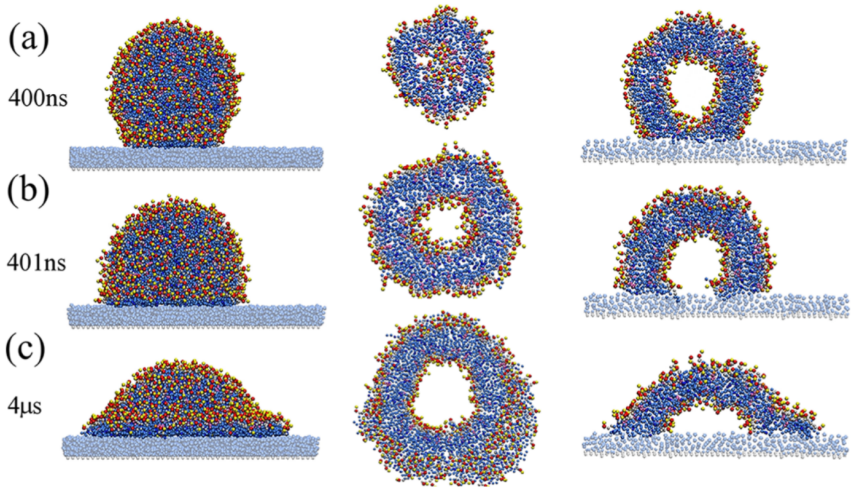

Figure 4.8: Snapshots from a coarse grained molecular dynamics simulation of a lipid vesicle adsorbing on a hydrophobic, oleophobic surface. Left column view from outside, middle column view on the vesicle parallel to the surface, right column perpendicular to the surface. Color code: lipid polar head- red and yellow, lipid nonpolar tail-blue. Water molecules not shown for transparency. The vesicle adsorbs on the surface, staying in a stable thimble-like structure. Adapted with permission from [55]. Copyright 2002 American Chemical Society.

4.1.3 Superspreading surfactant droplets

Of interest for the spreading observed in this work is also the phenomenon of *superspreading*. Superspreading surfactants are molecules which are able to make a water droplet on a hydrophobic surface spread rapidly and far (radius expands tenfold compared to initial value). It was first discovered in trisiloxane surfactants [57]. What has been long the subject of discussion was the reason, why some trisiloxanes form superspreading droplets and others do not.

Marangoni flow was long speculated to be the driving force of the superspreading, but recent works reviewed in [58] point at a different mechanism, called *rolling action*. They state that simply some trisiloxanes are able to push the spreading coefficient above zero $S = \gamma_{sg} - \gamma_{sl} - \gamma_{gl} > 0$ to total wetting and some not. Since the both trisiloxane classes can have similar γ_{gl}, the difference must be in γ_{sl}, the author of [58] claims. The difference is caused by the fact that the superspreading surfactants self-assemble to bilayers, while the non-superspreading ones to micelles. A micelle adsorbs to the water/surface interface as it is, staying in a 'blob', whereas a bilayer unzips on the surface, as was described in the above section. If the bilayers are concentrated enough, they form a continuous interface layer across the whole droplet, lessering γ_{sl} greatly and allowing spreading.

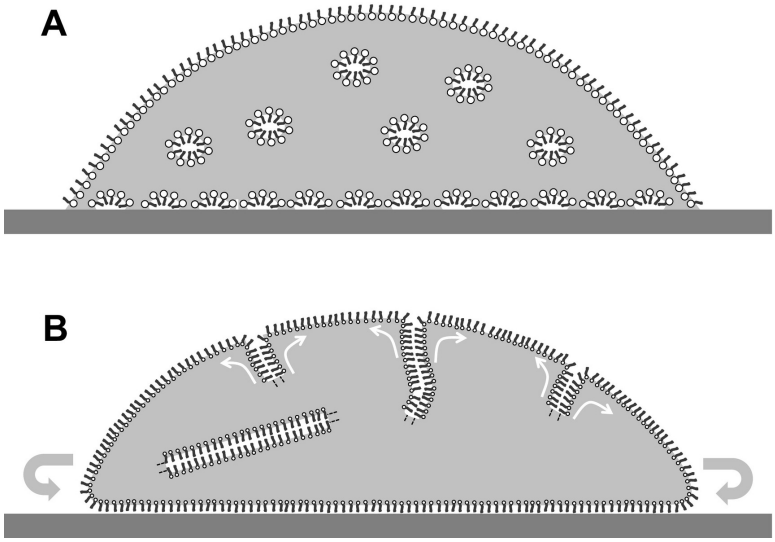

Figure 4.9: The proposed molecular explanation for the mechanism of superspreading and why some trisiloxane surfactants superspread and some do not. The superspreading (B) results from the formation a of continuous lipid monolayer, which rolls with the spreading droplet, being supplied from the unzipping dangling bilayers within the droplet. If the surfactants form micelles rather than bilayers (A), they cannot adsorb into a continous layer (on the timescale of superspreading) and the droplet does not superspread. Adapted with permission from [58]. Copyright 2021 Elsevier.

4.2 Possible explanations

4.2.1 Concentrated liposomes

The first explanation to the spreading of liposome-laden droplets that came to our mind was based on the observation that the liposomes act as surfactants, and that the surface tension γ_{gl} reduces with increasing concentration of the liposomes. As the droplet evaporates, the bulk concentration of liposomes rises, reducing γ_{gl} even more, which could lead to droplet spreading. In [20], a theoretical model for droplet evaporation and spreading was developed. It yielded a spreading of the droplet, similar to what we observed, which resulted from increasing bulk surfactant concentration.

As we see from Sec. 3.6.2, the liposomes themselves do not have any direct instantaneous effect on the surface tension. They have to adsorb on the droplet surface to reduce γ_{gl}, which takes time. The model in [20], however, assumes instantaneous adsorption of the surfactant on droplet surface. In our case, the instantaneous surface surfactant concentration is not in any case proportional to its instantaneous concentration in the bulk, and therefore we do not consider this model to be relevant for our problem.

4.2.2 DPPC as surfactant

In Sec. 4.1, we reviewed works where the effect of DPPC liposomes on γ_{gl} was discovered. To find out whether this tendency to decrease γ_{gl} could give rise to the observed droplet spreading, we proposed the following minimalistic theory.

Let us suppose γ_{gl} evolves with time in a sigmoid fashion similar to [16]:

$$\gamma_{gl} = 70 - \frac{A}{1 + \exp -[(t - t_0/)\tau]}, \tag{4.1}$$

where A is the magnitude of the liposome-induced tension change, t_0 is its characteristic timescale and τ its rapidity. This affects the static contact angle as well as the dynamic ones. These obey the formula:

$$\cos\theta_{A/R} = \frac{\gamma_{sg} - \gamma_{sl} \pm f}{\gamma_{gl}}, \tag{4.2}$$

where γ_{sg} is the surface tension of the surface/air interface, γ_{sl} for water/surface, γ_{gl} for air/water and f is the defect strength. As follows from the equation, the decrease of γ_{gl} can either increase an obtuse contact angle (static or dynamic) or decrease an acute one.

If both dynamic angles are acute, the situation can look as in Fig. 4.10 a): all the three angles suddenly decrease when the time t approaches the characteristic time scale t_0. The situation for parameters chosen to fit the droplet from Fig. 3.8 (blue) is in Fig. 4.11. It shows that the spreading of the droplet can result from the quick drop of θ_A. When $f > \gamma_{sg} - \gamma_{sl}$, the advancing contact angle becomes greater than 90°. In this case, the change of γ_{lg} makes it even greater, as can be seen in Fig. 4.10 b). According to this simple theory, spreading cannot occur for these parameters, as the transient angle cannot become higher than θ_A.

This simple theory therefore yields a mechanism for droplet spreading after the decrease of γ_{lg}, but only for advancing contact angles lesser than 90°.

The experimentally measured droplets assumed angles higher than 90° and still the spreading occurred, so we conclude that this theory alone cannot explain the phenomenon.

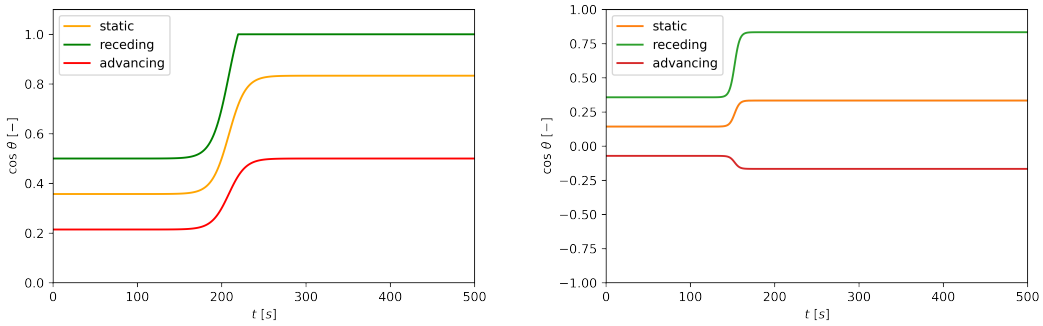

(a) (b)

Figure 4.10: Evolution of the cosine of the three contact angles for liposome-induced change of γ_{gl} for acute initial θ_A (a) and obtuse initial θ_A (b). The surface tension changes from $\gamma_{gl} = 70\text{mN/m}$ to 30mN/m with a characteristic time $t_0 = 200\text{s}$ and rapidity $\tau = 3\text{s}$. The values of $\gamma_{sg} - \gamma_{sl} = 25\text{mN/m}$ and $f = 10\text{mN/m}$ in (a) lead to $\theta(t = 0) = 69.1°$ and $\theta_A(t = 0) = 77.6°$. For (b) the values of $\gamma_{sg} - \gamma_{sl} = 10\text{mN/m}$ and $f = 15\text{mN/m}$ lead to $\theta_S(t = 0) = 81.8°$ and $\theta_A(t = 0) = 94.1°$. In both cases the range of allowed contact angles (between θ_A and θ_R) changes. The difference is that in (b) it only broadens, while for (a) it also shifts, meaning that some angles allowed before adsorption are not allowed after.

4.2.3 DPPC adsorbing on the surface

From the measured data it follows that liposome-laden droplets spread on the hydrophobic PTFE/Si surface, but not on the hydrophilic SiO_2. This suggests that the liposomes somehow interact with the surface.

As was discussed in Sec. 4.1.2, liposomes in suspensions adsorb to the surfaces they are in contact with, this hold for both hydrophilic and hydrophobic surfaces. For hydrophobic surfaces, the formation of monolayers was reported [53], which would surely decrease the surface energy between water and the hydrophobic surface. If γ_{sl} decreased in the evaporation process, one could get a dynamics similar as in Fig. 4.10 a). The example is shown in Fig. 4.12.

Apart from the nature of adsorption of the liposomes, there is also the question of the newly-formed contact area between the surface and the droplet that is formed when spreading: is the newlywet surface in contact with the water (surface energy γ_{sl0}) or with the adsorbed surfactant monolayer (γ_{sl1})?

In the first case, the energy added with the newlywet area δS is equal $\gamma_{sl0}\delta S$, as if the liposomes were not present at all. In the latter case it is equal to $\gamma_{sl1}\delta S$, and then the relevant quantity for the Young's relation is γ_{sl1}:

$$\cos\theta = \frac{\gamma_{sg} - \gamma_{sl1}}{\gamma_{lg}}. \tag{4.3}$$

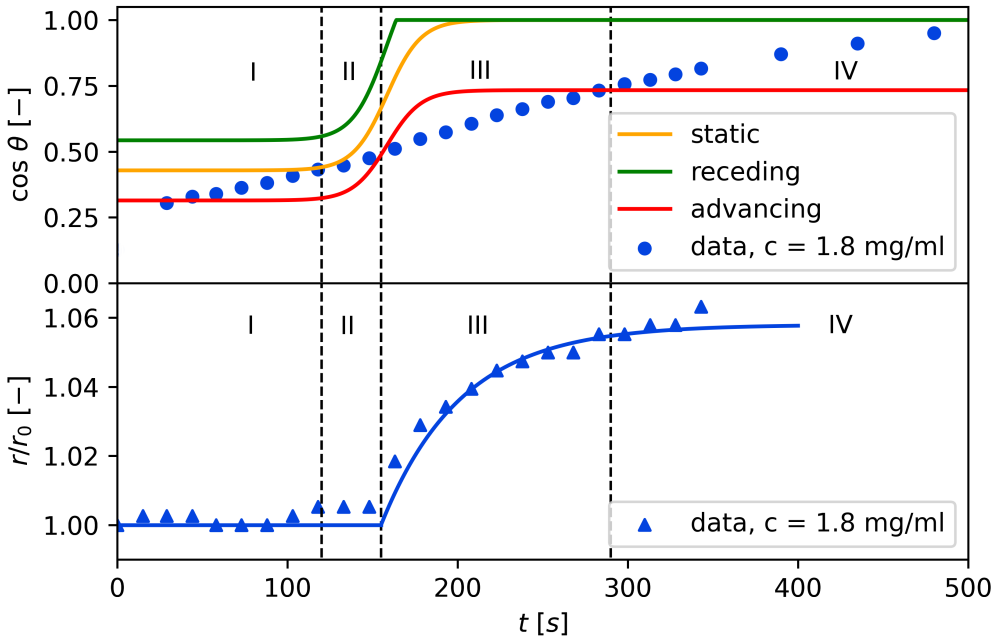

Figure 4.11: Spreading induced by liposomes adsorbing and lowering γ_{gl}. The upper graph shows the evolution of $\cos\theta$ for the three angles in the model and for experimental data taken from the droplet in Fig. 3.8 (blue). The lower part shows the relative radius for this droplet, the curve is a guide for the eye. The dynamics can be divided into four stages: (I) When the liposomes are being transported to the interface. They do not yet adsorb, so γ_{gl} and the angles are constant. No spreading occurs. (II) When the adsorption process happens, γ_{gl} decreases, lowering the three contact angles, until θ_A decreases and eventually reaches the instantaneous value of the droplet angle. (III) θ_A is now lower than the current droplet angle and the droplet tries to lower it by spreading. γ_{gl} and θ_A relax to a new equilibrum value. The droplet spreads, until the transient contact angle reaches θ_A again. (IV) Now the transient contact angle is between θ_A and θ_R and therefore no spreading occurs. The parameters of the model are $A = 40\text{mN/m}$, $t_0 = 150\text{s}$,$\tau = 10\text{s}$, $\gamma_{sg} - \gamma_{sl} = 30\text{mN/m}$ and $f = 8\text{mN/m}$. The initial contact angles are $\theta_S(t = 0) = 64.6°$ and $\theta_A(t = 0) = 71.7°$.

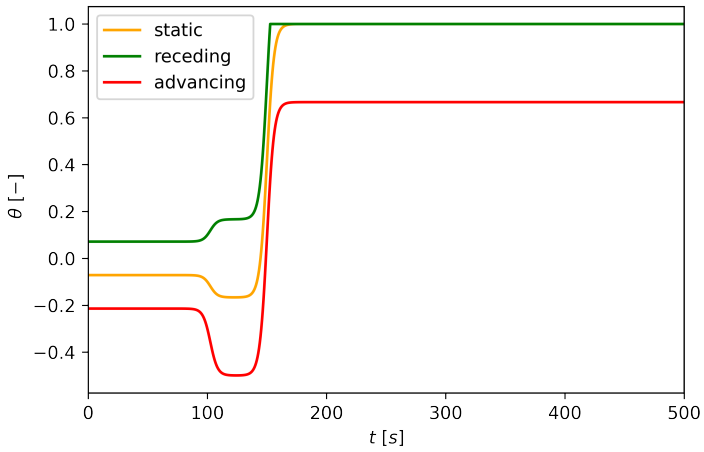

Figure 4.12: Evolution of the three contact angles . The surface tension changes from $\gamma_{gl} = 70\text{mN/m}$ to 30 with a characteristic time $t_0 = 100\text{s}$ and rapidity $\tau = 3\text{s}$. $\gamma_{sg} - \gamma_{sl0}$ changes from -5 to 30mN/m with a characteristic timescale $t_0 = 150\text{s}$ and rapidity $\tau = 3\text{s}$. $f = 10\text{mN/m}$. This models the surface turning from hydrophobic to hydrophilic upon adsorption. The contact angles react to this rapidly, θ_A changes from $\approx 120°$ to $\approx 50°$, allowing spreading.

The latter case would require some coordination from the side of the adsorbed DPPC, similar as in the case of superspreaders, see Fig. 4.9. As the liposomes adsorb to both the surface and the air interface, they may form a continuous layer that can roll out with the spreading contact line, as sketched in Fig. 4.13.

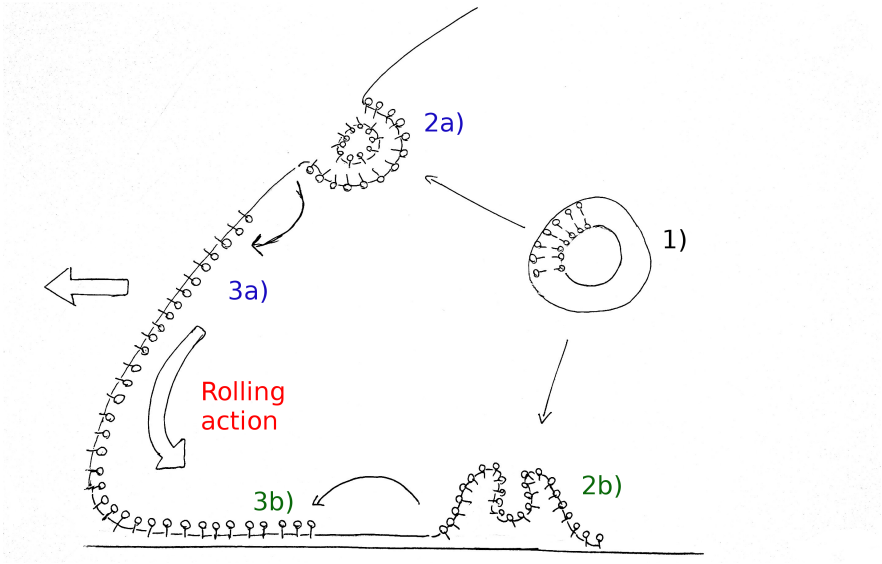

Figure 4.13: The proposed mechanism of droplet spreading. 1) The liposomes in the droplet are transported near one of the interfaces, where they adsorb and undergo conformation changes [2a) and 2b)]. 3) After reorganization, they form a lipid monolayer that spans from the water/surface interface to the air/water interface. This unrolls as the droplet spreads, so that the new water/surface contact is from the beginning bridged by the monolayer and the droplet feels lesser γ_{sl} from the new water/surface interface. In addition, also γ_{gl} is lessened.

The adsorption of the vesicles on the surfaces in the droplet has to be significantly affected by the flows within the droplet. Any deposited particle within an evaporating droplet can act as a defect, which can pin the contact line if it is transported there. The adsorbed liposomes surely do this too, however it is also likely that when they reorganize into monolayers, this effect is lessened, as the lipid monolayers are smooth and thin.

To support/disprove this hypothesis, we propose the following experiments :

1. Combine the measurement of droplet shape dynamics during evaporation with QCM measurements to see if the adsorption of the vesicles and reorganization of the adsorbed material somehow correlates with the onset of spreading.

2. Coat a PTFE/Si surface with DPPC suspension and investigate the adsorbed material with AFM, measure the contact angle of water on these surfaces.

3. Investigate the adsorption of the DPPC liposomes on the air/water surface in a similar fashion as in [44]: let a droplet of the suspension hang on a micropipette tip for a defined time and then drop on the surface and measure dynamics. If the vesicles adsorb on droplet surface while on a micropipette, it could start spreading right away after dropping.

4. Compare the dynamics of DPPC suspension droplets with the same concentration for unilamellar and multilamellar vesicles of the same size. Multilamellar vesicles are heavier and therefore should be slower in movement. When adsorbed, they have more layers to reorganize, therefore they should either not induce spreading or induce it in later times.

4.2.4 Why some droplets spread and others do not

The droplet shape dynamics measured is varies considerably from sample to sample. This can be seen in Fig. 3.8, where the three measured droplets with DPPC concentration 1.8mg/ml each behave differently: one does not spread at all, the second spreads from the beginning to almost the end and the third one starts spreading after 150s. It is possible, since we tracked the droplet shape only from one direction, that some droplets spread in the direction we did not track, but it is unlikely that the main part of the variance in the data is caused by this. Instead, it could be caused the following of reasons:

1. The surface is not homogenous on the scale of the contact line. The local strength of the defects pinning the contact line varies, which means that sometimes even when the mechanism which would allow the droplet to spread is active, it will not always spread, as sometimes the pinning from the defects is too strong.

2. The adsorption of vesicles is a stochastic process, which is self-averaged on the macroscopic scale. However, on the scale of the contact line again the randomness may produce significant deviations: two or more vesicles may merge into a large one that will act as a strong defect that can prevent

spreading, or vesicles can stack onto each other in a way such they cannot reorganize.

3. There could be a feedback mechanism between the adsorbed material and the flows within the droplet transport this material, which could result in an unstable behaviour triggering the spreading.

4.2.5 Timescales: transport or adsorption?

Another interesting question is what do the timescales upon which the droplets start spreading depend on mainly. According to our hypothesis of Sec. 4.2.3, the process leading to spreading can be divided into three steps:

1. transport (advection/diffusion) of the DPPC vesicle toward the interface,

2. adsorption of the vesicle on the interface,

3. unwrapping of the vesicle and formation of a surfactant monolayer.

The speed of the first step depends on evaporation rate, which is proportional to an external parameter that can be controlled in a thermostat: humidity. The speed of the second and third step could depend on liposome size, as smaller liposomes have greater curvature and could be harder to unwrap.

The way to test the contribution of these different rates is to to let the droplet evaporate at a much higher humidity ($\approx 90\%$) to slow down the advection (and extend droplet lifetime). One could then use different vesicle sizes and see whether the average spreading onset time depends on these parameters.

4.2.6 Late-stage protrusions

An interesting feature we observed in the microscope was the sudden formation of a protrusion on the contact line, seen in Fig. 4.14. This happened for a spreading 2mg/ml DPPC-laden droplet, when the contact line was already pinned.

The source of these protrusions could be the inverse micelles that float on the air/water surface following liposome adsorption. One micelle should be less than 100nm in diameter, but as [44] pointed out, these miceles can merge while on the interface. What happens when these micelles come into contact with the solid surface is not known, but since the non-polar tails of the surfactants point outward, it could adsorb and stick to the surface quickly and then merge with the rest of the droplet, creating the observed protrusion.

Another possible explanation is that as the coffee ring becomes thick it acts as an obstacle to the radial flow and the flow in turn pushes at the ring, driving it to some sort of buckling which results in the protrusion. This reasoning, however, does not explain why these protrusions are not present in droplets laden with ordinary nanoparticles. Alternatively, the protrusions could be caused by the same effect as the main droplet spreading, only now the effect is weakened.

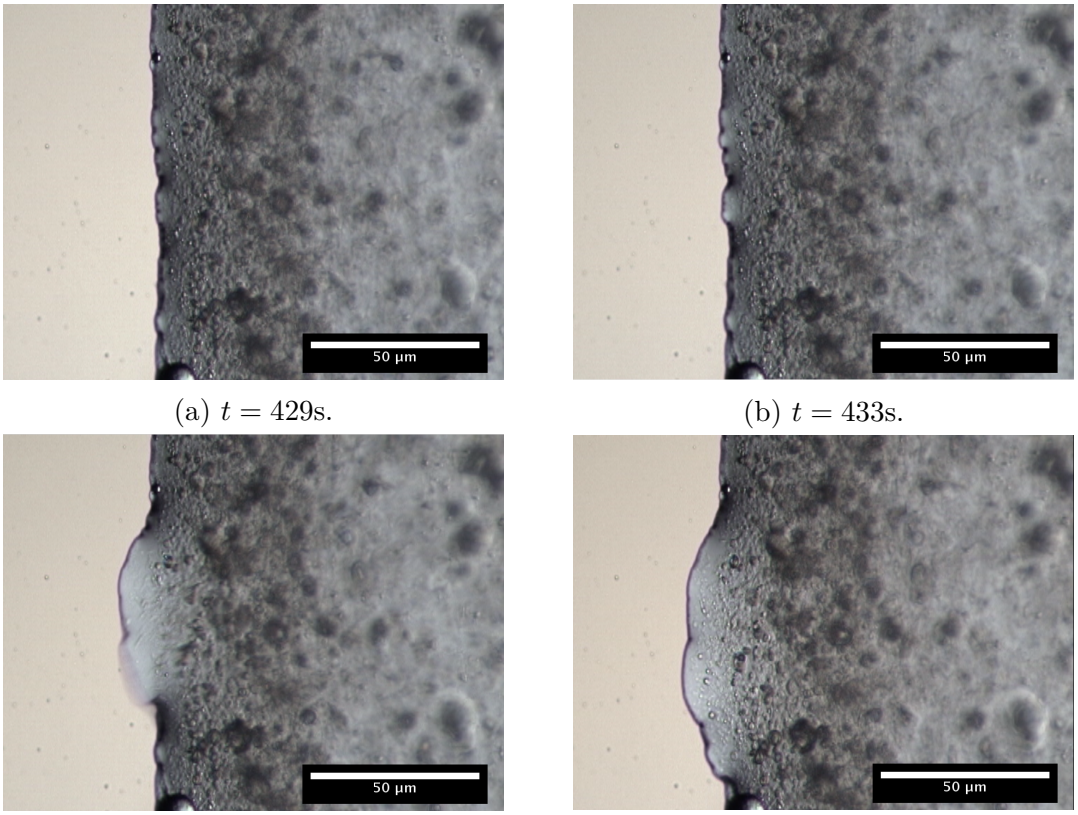

(a) $t = 429$s. (b) $t = 433$s.

(c) $t = 435$s. (d) $t = 437$s.

Figure 4.14: Sudden extension of a protrusion on the contact line in a 2μl droplet with DPPC suspension of concentration 2mg/ml. The droplet already stopped spreading and is pinned, a thick coffee ring of lipids (dark gray) is formed at the contact line (top). Then, suddenly, a protrusion extends from the contact line and stays like that (bottom).

Summary and outlook

In this thesis, we have discussed the interaction of sessile droplets with layered surfaces and the spreading of liposome-laden droplets.

Prolonged evaporation of penetrating droplets

We have shown how even a simple Teflon coated silicon wafer can be a very nontrivial surface for the droplet. With time the surface degrades and the droplet can penetrate it, burrowing under the top Teflon layer. The burrowed water is not exposed to the air and does not evaporate, causing the evaporation process to take remarkably long. We have observed this effect under the microscope and identified the characteristic patterns that form during the evaporation and that indicate penetration: growing wrinkles, pulsating fractal branches, undulating pockets, and the formation of an outer ring far beyond the droplet contact diameter.

This behaviour was, to our knowledge, never reported before and presents a new simple method to test the stability of thin films. The discovered instability of plasma Teflon coatings merits the questions of when exactly do the films start being unstable and what can be done to improve the stability. This could be tested by observing the evaporation on surfaces of varying age and for different manufacturing protocols.

Spreading of liposome-laden droplets

We have investigated the spreading of liposome-laden droplets in a quantitative fashion and found some of them undergo abrupt transition from a being pinned to spreading, with final droplet diameter up to 1.3-times larger than the initial one. However, not all droplets behave the same, even if initiated with the same macroscopic conditions (liposome concentration, surface, temperature, humidity, droplet volume). Some spread and some do not, which we attribute to random defect of the surface which becomes relevant on the scale of the contact line.

We have reviewed works dealing with liposome adsorption on interfaces and their effect on surface tension. As the liposome vesicles need to reorganize their shape to adsorb, this process is slow enough to happen on timescales similar to that of the droplet spreading observed. We further devise two simple models incorporating this adsorption. The first model only considers the adsorption on the air/water interface, the second one also on the water/surface interface. We show that the first simpler model cannot robustly explain the observed spreading, but the second one can. Finally, we propose experiments able to support or disprove the validity of the second model: (i) Correlating the onset of droplet spreading with QCM measurements to find out the role of liposome surface adsorption in the spreading. (ii) Compare the deposits of spreading and non-spreading droplets with AFM to see if there are visible differences in the adsorbed vesicles. (iii) Investigate the adsorption to the air/water interface by letting the droplet first equilibrate on a micropipette tip, then dropping it and observing the evaporation process, to see whether will the droplet now spread sooner (iv) Testing for different liposome vesicle topologies to see how differently adsorbing vesicles alter the spreading.

Bibliography

[1] R. G. Larson. "Transport and deposition patterns in drying sessile droplets". en. In: *American Institute of Chemical Engineers Journal* 60.5 (May 2014), pp. 1538–1571.

[2] H. Wijshoff. "Drop dynamics in the inkjet printing process". In: *Current Opinion in Colloid and Interface Science* 36 (2018). Wetting and Spreading, pp. 20–27. ISSN: 1359-0294.

[3] J. L. Garcia-Cordero and Z. H. Fan. "Sessile droplets for chemical and biological assays". In: *Lab on a Chip* 17 (13 2017), pp. 2150–2166.

[4] M. A. Ray, H. Kim, and L. Jia. "Dynamic Self-Assembly of Polymer Colloids To Form Linear Patterns". In: *Langmuir* 21.11 (2005). PMID: 15896010, pp. 4786–4789.

[5] R. Bhardwaj, X. Fang, P. Somasundaran, and D. Attinger. "Self-Assembly of Colloidal Particles from Evaporating Droplets: Role of DLVO Interactions and Proposition of a Phase Diagram". In: *Langmuir* 26.11 (2010). PMID: 20337481, pp. 7833–7842.

[6] A. Kuižová, M. Přikryl, M. Procázka, and E. Kočišová. "Drop coating deposition Raman (DCDR) spectroscopy of contaminants". In: *Spectrochimica Acta Part A: Molecular and Biomolecular Spectroscopy* 262 (2021), p. 120109. ISSN: 1386-1425.

[7] D. Zhang, Y. Xie, M. F. Mrozek, C. Ortiz, V. J. Davisson, and D. Ben-Amotz. "Raman Detection of Proteomic Analytes". In: *Analytical Chemistry* 75.21 (2003). PMID: 14588009, pp. 5703–5709.

[8] Jung and H.-Y. Kwak. "Separation of Microparticles and Biological Cells Inside an Evaporating Droplet Using Dielectrophoresis". In: *Analytical Chemistry* 79.13 (2007). PMID: 17523596, pp. 5087–5092.

[9] N. Kim, Z. Li, C. Hurth, F. Zenhausern, S.-F. Chang, and D. Attinger. "Identification of fluid and substrate chemistry based on automatic pattern recognition of stains". In: *Analytical Methods* 4 (1 2012), pp. 50–57.

[10] P. de Gennes, F. Brochard-Wyart, and D. Quere. *Capillarity and Wetting Phenomena: Drops, Bubbles, Pearls, Waves*. Springer New York, 2004. ISBN: 978-0-387-21656-0.

[11] H. Hu and R. G. Larson. "Evaporation of a Sessile Droplet on a Substrate". In: *The Journal of Physical Chemistry B* 106.6 (2002), pp. 1334–1344.

[12] R. D. Deegan, O. Bakajin, T. F. Dupont, G. Huber, S. R. Nagel, and T. A. Witten. "Capillary flow as the cause of ring stains from dried liquid drops". In: *Nature* 389.6653 (Oct. 1997), pp. 827–829. ISSN: 1476-4687.

[13] H. Hu and R. G. Larson. "Analysis of the Effects of Marangoni Stresses on the Microflow in an Evaporating Sessile Droplet". In: *Langmuir* 21.9 (2005). PMID: 15835963, pp. 3972–3980.

[14] H. Hu and R. G. Larson. "Marangoni Effect Reverses Coffee-Ring Depositions". In: *The Journal of Physical Chemistry B* 110.14 (2006). PMID: 16599468, pp. 7090–7094.

[15] M. Drábik, O. Polonskyi, O. Kylián, J. Čechvala, A. Artemenko, I. Gordeev, A. Choukourov, D. Slavínská, I. Matolínová, and H. Biederman. "Super-Hydrophobic Coatings Prepared by RF Magnetron Sputtering of PTFE". In: *Plasma Processes and Polymers* 7.7 (2010), pp. 544–551.

[16] X. Wen and E. I. Franses. "Role of Subsurface Particulates on the Dynamic Adsorption of Dipalmitoylphosphatidylcholine at the Air/Water Interface". In: *Langmuir* 17.11 (2001), pp. 3194–3201.

[17] A. Pinazo, X. Wen, Y.-C. Liao, A. J. Prosser, and E. I. Franses. "Comparison of DLPC and DPPC in Controlling the Dynamic Adsorption and Surface Tension of Their Aqueous Dispersions". In: *Langmuir* 18.23 (2002), pp. 8888–8896.

[18] B. Seantier, C. Breffa, O. Félix, and G. Decher. "Dissipation-Enhanced Quartz Crystal Microbalance Studies on the Experimental Parameters Controlling the Formation of Supported Lipid Bilayers". In: *The Journal of Physical Chemistry B* 109.46 (2005). PMID: 16853826, pp. 21755–21765.

[19] T. A. Nguyen, S. Biggs, A. Doi, and A. V. Nguyen. "A new way of assessing droplet evaporation independently of the substrate hydrophobicity and contact line mode: A case study of sessile droplets with surfactants". In: *Colloids and Surfaces A: Physicochemical and Engineering Aspects* 577 (2019), pp. 396–404. ISSN: 0927-7757.

[20] M. Wu, Y. Di, X. Man, and M. Doi. "Drying Droplets with Soluble Surfactants". In: *Langmuir* 35.45 (2019). PMID: 31604016, pp. 14734–14741.

[21] X. Shao, F. Duan, Y. Hou, and X. Zhong. "Role of surfactant in controlling the deposition pattern of a particle-laden droplet: Fundamentals and strategies". In: *Advances in Colloid and Interface Science* 275 (2020), p. 102049. ISSN: 0001-8686.

[22] J. González-Gutiérrez, R. Pérez-Isidoro, M. Pérez-Camacho, and J. Ruiz-Suárez. "The calorimetric properties of liposomes determine the morphology of dried droplets". In: *Colloids and Surfaces B: Biointerfaces* 155 (2017), pp. 215–222. ISSN: 0927-7765.

[23] *Capillary length Wikipedia page*. `https://en.wikipedia.org/wiki/Capillary_length`. Accessed: 2022-04-13.

[24] T. S. Physics. *Microdroplets vs macrodroplets Wikipedia page*. `https://commons.wikimedia.org/wiki/File:Sessile_drop_Capillary_Length.jpg`. Accessed: 2022-04-13.

[25] G. McHale, N. J. Shirtcliffe, and M. I. Newton. "Contact-Angle Hysteresis on Super-Hydrophobic Surfaces". In: *Langmuir* 20.23 (2004). PMID: 15518506, pp. 10146–10149.

[26] A. F. Stalder, T. Melchior, M. Müller, D. Sage, T. Blu, and M. Unser. "Low-bond axisymmetric drop shape analysis for surface tension and contact angle measurements of sessile drops". In: *Colloids and Surfaces A: Physicochemical and Engineering Aspects* 364.1 (2010), pp. 72–81. ISSN: 0927-7757.

[27] A. Stalder, G. Kulik, D. Sage, L. Barbieri, and P. Hoffmann. "A snake-based approach to accurate determination of both contact points and contact angles". In: *Colloids and Surfaces A: Physicochemical and Engineering Aspects* 286.1 (2006), pp. 92–103. ISSN: 0927-7757.

[28] E. B. I. Group. *EPFL Biomedical Imaging Group Drop Analysis page*. `http://bigwww.epfl.ch/demo/dropanalysis`. Accessed: 2022-04-28.

[29] J. K. Park, J. Ryu, B. C. Koo, S. Lee, and K. H. Kang. "How the change of contact angle occurs for an evaporating droplet: effect of impurity and attached water films". In: *Soft Matter* 8 (47 2012), pp. 11889–11896.

[30] "Theoretical and experimental analysis of droplet evaporation on solid surfaces". In: *Chemical Engineering Science* 69.1 (2012), pp. 522–529. ISSN: 0009-2509.

[31] S. Jafari Kang, V. Vandadi, J. D. Felske, and H. Masoud. "Alternative mechanism for coffee-ring deposition based on active role of free surface". In: *Physical Review E* 94 (6 Dec. 2016), p. 063104.

[32] R. D. Deegan. "Pattern formation in drying drops". In: *Phys. Rev. E* 61 (1 Jan. 2000), pp. 475–485.

[33] M. Moore, D. Vella, and J. Oliver. "The nascent coffee ring: how solute diffusion counters advection". In: *Journal of Fluid Mechanics* 920 (2021), A54.

[34] T. A. H. Nguyen and A. V. Nguyen. "On the Lifetime of Evaporating Sessile Droplets". In: *Langmuir* 28.3 (2012). PMID: 22239111, pp. 1924–1930.

[35] T. A. H. Nguyen and A. V. Nguyen. "Increased Evaporation Kinetics of Sessile Droplets by Using Nanoparticles". In: *Langmuir* 28.49 (2012). PMID: 23171287, pp. 16725–16728.

[36] J. Y. Kim and B. M. Weon. "Evaporation of strong coffee drops". In: *Applied Physics Letters* 113.18 (2018), p. 183704.

[37] P. Bryk, E. Korczeniewski, G. S. Szymański, P. Kowalczyk, K. Terpiłowski, and A. P. Terzyk. "What Is the Value of Water Contact Angle on Silicon?" In: *Materials* 13.7 (2020). ISSN: 1996-1944.

[38] A. Kuižová, A. Kuzminova, O. Kylián, and E. Kočišová. "Nanostructured Plasma Polymerized Fluorocarbon Films for Drop Coating Deposition Raman Spectroscopy (DCDRS) of Liposomes". In: *Polymers* 13.22 (2021). ISSN: 2073-4360.

[39] E. Kočišová and M. Procházka. "Drop-coating deposition Raman spectroscopy of liposomes". In: *Journal of Raman Spectroscopy* 42.8 (2011), pp. 1606–1610.

[40] W. Stillwell. *An introduction to biological membranes*. London, England: Elsevier Science, May 2013.

[41] A. Kuižová. *Ramanova spektroskopia kvapkovo nanášaných povlakov biologicky významných molekúl*. Univerzita Karlova, Matematicko-fyzikální fakulta, Fyzikální ústav UK, Sept. 2019.

[42] P. RNDr. Pavel Solař. *Solarius Software webpage*. `http://solarius-software.sweb.cz`. Accessed: 2022-05-03.

[43] C.-H. Chang, K. A. Coltharp, S. Y. Park, and E. I. Franses. "Surface tension measurements with the pulsating bubble method". In: *Colloids and Surfaces A: Physicochemical and Engineering Aspects* 114 (1996), pp. 185–197. ISSN: 0927-7757.

[44] X. Bai, L. Xu, J. Y. Tang, Y. Y. Zuo, and G. Hu. "Adsorption of Phospholipids at the Air-Water Surface". In: *Biophysical Journal* 117.7 (2019), pp. 1224–1233. ISSN: 0006-3495.

[45] S. M. I. Saad, Z. Policova, E. J. Acosta, and A. W. Neumann. "Axisymmetric Drop Shape AnalysisConstrained Sessile Drop (ADSA-CSD): A Film Balance Technique for High Collapse Pressures". In: *Langmuir* 24.19 (2008). PMID: 18759471, pp. 10843–10850.

[46] R. Richter, A. Mukhopadhyay, and A. Brisson. "Pathways of Lipid Vesicle Deposition on Solid Surfaces: A Combined QCM-D and AFM Study". In: *Biophysical Journal* 85.5 (Nov. 2003), pp. 3035–3047.

[47] Z. Wang and S. Yang. "Adsorption Behaviors of DPPC/MO Aggregates on SiO2 Surfaces". In: *Langmuir* 24.20 (2008). PMID: 18763819, pp. 11616–11624.

[48] B. Ramm, P. Glock, and P. Schwille. "In Vitro Reconstitution of Self-Organizing Protein Patterns on Supported Lipid Bilayers". In: *Journal of Visualized Experiments* 137 (July 2018), e58139. ISSN: 1940-087X.

[49] L. Kam and S. G. Boxer. "Spatially Selective Manipulation of Supported Lipid Bilayers by Laminar Flow: Steps Toward Biomembrane Microfluidics". In: *Langmuir* 19.5 (2003), pp. 1624–1631.

[50] *Model lipid bilayer Wikipedia page*. `https://en.wikipedia.org/wiki/Model_lipid_bilayer`. Accessed: 2022-04-06.

[51] Y. Jing, H. Trefna, M. Persson, B. Kasemo, and S. Svedhem. "Formation of supported lipid bilayers on silica: relation to lipid phase transition temperature and liposome size". In: *Soft Matter* 10 (1 2014), pp. 187–195.

[52] MDougM. *Supported bilayer Wikipedia image*. `http://commons.wikimedia.org/wiki/File:Supported_bilayer.svg`. Accessed: 2022-04-06.

[53] S. Lingler, I. Rubinstein, W. Knoll, and A. Offenhäusser. "Fusion of Small Unilamellar Lipid Vesicles to Alkanethiol and Thiolipid Self-Assembled Monolayers on Gold". In: *Langmuir* 13.26 (1997), pp. 7085–7091.

[54] C. Keller and B. Kasemo. "Surface Specific Kinetics of Lipid Vesicle Adsorption Measured with a Quartz Crystal Microbalance". In: *Biophysical Journal* 75.3 (1998), pp. 1397–1402. ISSN: 0006-3495.

[55] I. Mannelli, F. Sagués, V. Pruneri, and R. Reigada. "Lipid Vesicle Interaction with Hydrophobic Surfaces: A Coarse-Grained Molecular Dynamics Study". In: *Langmuir* 32.48 (2016). PMID: 27808519, pp. 12632–12640.

[56] C. Kataoka-Hamai and K. Kawakami. "Interaction Mechanisms of Giant Unilamellar Vesicles with Hydrophobic Glass Surfaces and Silicone Oil–Water Interfaces: Adsorption, Deformation, Rupture, Dynamic Shape Changes, Internal Vesicle Formation, and Desorption". In: *Langmuir* 35.49 (2019). PMID: 31697503, pp. 16136–16145.

[57] K. Ananthapadmanabhan, E. Goddard, and P. Chandar. “A study of the solution, interfacial and wetting properties of silicone surfactants”. In: *Colloids and Surfaces* 44 (1990), pp. 281–297. ISSN: 0166-6622.

[58] J. Venzmer. “Superspreading – Has the mystery been unraveled?” In: *Advances in Colloid and Interface Science* 288 (2021), p. 102343. ISSN: 0001-8686.

A. Attachments

A.1 Source code of droplet shape automatic fitting script

```
1
2 #Script auto_dropsnake.py
3 #This script uses the pyautogui and sys python packages
4 #it manipulates ImageJ and its DropAnalysis plugin
5 #so both have to be installed.
6 #Drop Analysis can be downloaded at
7 #http://bigwww.epfl.ch/demo/dropanalysis/
8
9 #the positions in the script are valid for screen resolution 1600
    x900,
10 #so change your screens resolution to this value
11
12 #to analyze the droplet shape for a given sequence of images
13 #open ImageJ, open the sequence using File-> Import-> Sequence
14 #crop the sequence, keeping only the area around the droplet
15 #then turn sequence to grayscale (Image->Type->8bit)
16
17 #now open Plugins-> drop_analysis-> Drop Snake
18 #you must fit the initial image yourself
19
20 #you can choose the first image of the sequence and then proceed
21 #to later frames (forward mode) or
22 #an image later in the sequence and proceed to earlier frames (
    backward mode).
23 # Choose the mode by uncommenting the respective line in the code
24
25 #detailed instructions for the fitting are in the pdf in the plugin
    directory
26 #in short: create the knots around the droplet edge as described
27 #then click the Snake button, which should fit the droplet correctly
28 #if it did, click Accept (green triangle)
29
30 #you could proceed like this through the whole sequence
31 #but this algorithm can do it for you!
32 #what it does is, it clicks the buttons automatically
33 #you must move the ImageJ menu to the top right corner of the screen
34 #and the droplet window somewhere beneath it
35
36 #then you can run the script in command line with:
37 # python auto_dropsnake.py {FITNUM}
38 #(change {FITNUM} for the number of frames you want the script to
    fit)
39 #it is not recommended to fit droplets with CA lower than 20,
40 #as the tilt of the surface interferes with the results
41 #Export your data results to .txt file in the Final Curves window
42
43 #Happy fitting!
44
45 #Copyright Juraj Majek, KMF MFF UK, 2022
46
```

```
47 import pyautogui
48 import sys
49
50 N = sys.argv[1]
51
52 for i in range(1,N):
53
54
55     #now the algorithm proceeds to the next image in sequence
56
57     pyautogui.click(1164, 45) #image
58     pyautogui.click(1164, 169) #stacks
59
60     #uncomment one of these lines
61     #pyautogui.click(1386, 210) #forward mode
62     #pyautogui.click(1355, 231) #backward mode
63
64
65     #fit the current image
66     pyautogui.click(1196, 68)
67
68     #some mouse moves to reload image on display
69     pyautogui.moveTo(1111, 140, duration=0.01)
70     pyautogui.moveTo(1111, 520, duration=0.01)
71     pyautogui.moveTo(1243, 13, duration=0.01)
72
73     #save current fit
74     pyautogui.click(1220, 66)
75     #confirm saving
76     pyautogui.click(800, 233)
```